Materials Today Bio 27 (2024) 101159

Contents lists available at ScienceDirect

Materials Today Bio

journal homepage: www.journals.elsevier.com/materials-today-bio

Glucose-responsive, self-healing, wet adhesive and multi-biofunctional hydrogels for diabetic wound healing

Zhuo Huang [a,1], Min Wang [a,1], Langjie Chai [a], Hang Chen [a], Danyang Chen [a], Yulin Li [b], Hongtao Liu [c], You Wu [c], Xuxia Yang [c], Lu He [a], Longjian Xue [c], Yifeng Lei [c,d,**], Liang Guo [a,*]

[a] Department of Plastic Surgery, Zhongnan Hospital of Wuhan University, Wuhan, 430071, China
[b] The Emergency Center, Zhongnan Hospital of Wuhan University, Wuhan, 430071, China
[c] The Institute of Technological Science & School of Power and Mechanical Engineering, Wuhan University, Wuhan, 430072, China
[d] Wuhan University Shenzhen Research Institute, Shenzhen, 518057, China

ARTICLE INFO

Keywords:
Diabetic wound healing
Hydrogel
Wet adhesion
Self-healing
Glucose-responsive release

ABSTRACT

Diabetic wounds are serious clinical complications which manifest wet condition due to the mass exudate, along with disturbed regulation of inflammation, severe oxidative stress and repetitive bacterial infection. Existing treatments for diabetic wounds remain unsatisfactory due to the lack of ideal dressings that encompass mechanical performance, adherence to moist tissue surfaces, quick repair, and diverse therapeutic benefits. Herein, we fabricated a wet adhesive, self-healing, glucose-responsive drug releasing hydrogel with efficient antimicrobial and pro-healing properties for diabetic wound treatment. PAE hydrogel was constructed with poly(acrylic acid-*co*-acrylamide) (AA-Am) integrated with a dynamic E-F crosslinker, which consisted of epigallocatechin gallate (EGCG) and 4-(2-acrylamidoethylcarbamoyl)-3-fluorophenylboronic acid (AFPBA). Due to the dynamic crosslinking nature of boronate esters, abundant catechol groups and hydrogen bonding, PAE hydrogel demonstrated excellent mechanical properties with about 1000 % elongation, robust adhesion to moist tissues, fast self-healing, and absorption of biofluids of 10 times of its own weight. Importantly, PAE hydrogel exhibited sustained and glucose-responsive release of EGCG. Together, the bioactive PAE hydrogel had effective antibacterial, antioxidative, and anti-inflammatory properties *in vitro*, and accelerated diabetic wound healing in rats via reducing tissue-inflammatory response, enhancing angiogenesis, and reprogramming of macrophages. Overall, this versatile hydrogel provides a straightforward solution for the treatment of diabetic wound, and shows potential for other wound-related application scenarios.

1. Introduction

Diabetes stands out as a widespread and rapidly rising global chronic disease, with 19%–34 % of diabetic patients potentially developing diabetic wounds [1]. These medical complications have severe consequences, including necessitating amputations of the lower extremities [2]. The hallmarks of diabetic wounds include ongoing bacterial infections, elongated inflammation periods, excessive oxidative stress, disrupted angiogenesis, and an overabundance of wound exudates that contribute to extended healing time or even non-healing instances [3,4]. Modern treatment approaches, such as antimicrobial therapies, traditional wound dressings (gauze, cotton pads and bandages), and negative pressure wound therapy, are unable to adequately mitigate these complex pathological pathways, thereby yielding an unsatisfying success rate [3,4]. Thus, there is an urgent need for more potent interventions to adequately target this significant health concern.

An approach that holds considerable promise in diabetic wound therapy is the utilization of novel wound dressing. Numerous multifunctional materials have been developed for wound healing application [5,6], integrating different bioactive components in various forms such as sponges, nanofibers, and hydrogels [7–10]. Among them, intelligent hydrogels have attracted emerging attention in diabetic wound healing due to their excellent properties [11], such as real-time monitoring, stimuli-responsiveness (including glucose-responsiveness), self-healing,

* Corresponding author. Department of Plastic Surgery, Zhongnan Hospital of Wuhan University, Wuhan, 430071, China
** Corresponding author. The Institute of Technological Science & School of Power and Mechanical Engineering, Wuhan University, Wuhan, 430072, China.
E-mail addresses: yifenglei@whu.edu.cn (Y. Lei), guolianghbwh@163.com (L. Guo).
[1] These authors contributed equally to this work.

https://doi.org/10.1016/j.mtbio.2024.101159
Received 15 April 2024; Received in revised form 5 July 2024; Accepted 15 July 2024
Available online 19 July 2024

wet tissue adhesion, on-demand drug release, and so on [12,13]. Meanwhile, hydrogels are also encapsulated with biological regulatory functions, including reactive oxygen species neutralization, immunomodulatory, and antimicrobial activity [14–16]. As promising as these advances, existing hydrogel dressing remain unsatisfactory, due to the lack of ideal dressings that can encompass superior mechanical performance, wet tissue adhesion, quick repair, and glucose-responsive drug release together.

Acrylic acid (AA) and acrylamide (Am) are among the main materials used in the synthesis of hydrogels [16,17]. Poly (acrylic acid--*co*-acrylamide) (AA-Am) hydrogels can be synthesized by free-radical polymerization in mild condition [18], and have been widely applied in wound dressing [19]. Unfortunately, the poor adhesion under wet condition, lack of glucose-responsive release property has limited its use in diabetic wound dressings.

In nature, living organisms such mussel, barnacles, spider glue exhibit a powerful wet adhesive ability due to the elegant blend of catechol chemistry and supramolecular structures [20–22]. Moreover, plant-inspired polyphenol-containing materials show good tissue adhesion and self-healing capacity [23,24]. Which were widely used for developing wet tissue adhesives [25–27]. Among these polyphenols, epigallocatechin gallate (EGCG), the major active compound in green tea, could not only enhance wet adhesion [23], but also exhibits potent anti-inflammatory, antioxidant and antibacterial activities [28,29]. Given these beneficial bioactivities, the integration of EGCG within AA-Am hydrogels appear well suitable for wound dressing, with effective wet adhesion ability and favorable therapeutic effects. Moreover, due to the hyperglycemia in diabetes, glucose-responsive releasing system is advantageous for sustained drug release in diabetic wound healing [30].

Based on this consideration, herein, we developed a multifunctional hydrogel wound dressing with satisfactory wet adhesion, fast self-healing and glucose-responsive drug release, by utilizing a simple reaction method to copolymerize AA-Am with a dynamic E-F crosslinker (Fig. 1), where the latter consisted of EGCG binding with 4-(2-acrylamidoethylcarbamoyl)-3-fluorophenylboronic acid (AFPBA) (Fig. 1A). The AA-Am backbone and E-F crosslinker were crosslinked via radical polymerization (Fig. 1A–C). The obtained PAE hydrogel with dynamic boronate esters, free catechol groups, and abundant hydrogen bonding, possessed flexibility, rapid self-healing, and wet tissue adhesion abilities, which provided long-term protection for wound dressing against body movement and external stress. PAE hydrogel can absorb considerable amounts of extrudates, which promotes effective drainage of diabetic wound. More importantly, PAE hydrogel can glucose-responsively and continuously release EGCG molecules, therefore exhibited antimicrobial, antioxidative, and anti-inflammatory activities, and accelerated diabetic wound healing through promoting angiogenesis, reducing inflammatory response and regulating macrophage polarization (Fig. 1D).

2. Materials and methods

2.1. Materials

EGCG (95 %), AA (99 %), Am (99 %), ammonium persulfate (APS, 98.5 %), N, N, N′, N′-tetramethylethylenediamine (TEMED, 99 %) and dimethyl sulfoxide (DMSO, 99 %) were purchased from Shanghai Aladdin Biochemical Technology Co., Ltd. AFPBA (95 %) was obtained from Bide Pharmatech Co., Ltd.

2.2. Synthesis of PAE hydrogel

E-F crosslinker was formed based on the reversible binding of phenylboronic acid with the diol group to form a cyclic boronate (Fig. 1A). In brief, EGCG was dissolved in dimethyl sulfoxide (DMSO) at a concentration of 0.4 M, and AFPBA was added in DMSO at a concentration of 0.8 M. The solutions were mixed at a volume ratio of 1:1 and reacted for 15 min at room temperature. The molar ratio of AFPBA to EGCG was designed as 2:1 for complete reaction of AFPBA (Fig. 1A).

PAE hydrogels were synthesized by radical copolymerization of E-F

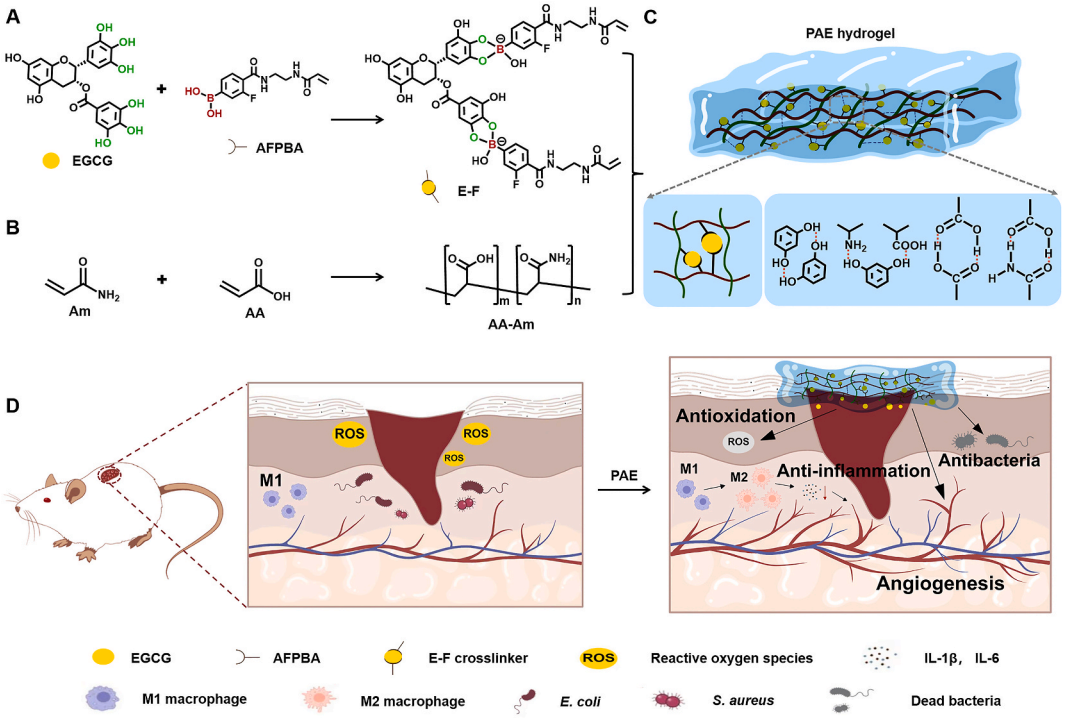

Fig. 1. Schematic illustration of the synthesis of PAE hydrogel for diabetic wound healing. (A) Illustration of the formation of E-F dynamic crosslinker. (B) Illustration of crosslinking of AA-Am hydrogel. (C) Illustration of crosslinking of PAE hydrogel via radical polymerization and hydrogen bonding. (D) Illustration of multiple therapeutic effects of PAE hydrogel to accelerate diabetic wound healing.

crosslinker and AA-Am precursor solution (Fig. 1A–C). Briefly, 1.7 g Am (2.4 M) was dissolved in 10 mL water, then mixed with 1.3 mL AA till fully dissolution. AA-Am precursor solution was formed following the addition of 0.2 g APS and 75 μL TEMED according to previous report [31]. Subsequently, the AA-Am precursor solution was mixed with the above prepared E-F crosslinker with different concentrations. The mixture was then poured into a closed glass mold, degassed, and placed in a 60 °C heater for crosslinking, to obtain the PAE hydrogel (Fig. 1C). The gelation time was determined by inversing the mixture at room temperature. PAE hydrogels with different concentration of E-F crosslinker (3, 5 and 8 mM) were named as PAE 3, PAE 5 and PAE 8, respectively. For the *in vitro* and *in vivo* experiments involving in the use of PAE hydrogels or PAE hydrogel extract, the hydrogels were first immersed in ethanol and then washed in fresh phosphate-buffered saline (PBS, pH = 7.4), and this process was replicated for 3 times to remove the unreacted compounds.

2.3. Physicochemical characterization

The status and appearance of the hydrogels were monitored by high-resolution cell phone (Apple iPhone XR). Sectional morphology of the AA-Am and PAE hydrogels were observed by scanning electron microscope (SEM, Zeiss SIGMA). The elemental composition and chemical structure of the hydrogels were analyzed by X-ray photoelectron spectroscopy (XPS, Thermo Fisher ESCA-LAB 250XI) and Fourier transform infrared spectroscopy (FTIR, Thermo Fisher NICOLET6700), respectively.

2.4. Mechanical property test

Mechanical properties of the hydrogels were analyzed using a universal testing machine (UTM2503, Shenzhen Suns Technology). In tensile tests, samples were made into dumbbell shape with a length of 50 mm and a section size of 4 mm × 2 mm, and the tensile speed was set as 20 mm min^{-1}. In compression tests, samples were made into cylindrical shape with a height of 8 mm and a section diameter of 15 mm, and the compression speed was set as 2 mm min^{-1}. All tests were repeated for 5 times.

In addition, bending, compressing and twisting of the hydrogels were performed with fingers. Meanwhile, a round shaped hydrogel was stretched by two tweezers in opposite directions, to test the elasticity and elongation of the hydrogel. Furthermore, a rectangle shaped hydrogel was attached to finger joint, to test the adhesiveness and deformability of the hydrogel. All human body related experiments of on-skin tests on volunteers were performed under approval by the Biomedical Ethics Committee of Wuhan University (2022090).

2.5. Rheological property test

The rheological property test of the hydrogels was carried out on a rheometer (Kinexus lab+, Malvern). The storage modulus (G′) and loss modulus (G″) were investigated by placing the hydrogels on a parallel plate with a 25 mm diameter. Strain amplitude sweep tests (γ = 0.1 %–1000 %) were carried out at 37 °C to detect the critical strain point of the hydrogels. Then, G′ and G″ of hydrogels during five cycles of oscillation strain between 1 % and 1200 % were measured with a 1 Hz frequency at 37 °C.

2.6. Adhesion and wet adhesion test

Fresh porcine tissues including skin, muscle, kidney and liver were obtained from nearby fresh market. All tissues were cut into 6 cm × 3 cm sheets, and a 1 cm-diameter round defect was created in the center by biopsy punch. Then a round PAE hydrogel with a diameter of 2.5 cm was applied on top of the defect area for 3 min. Afterwards, the push-out test was conducted manually to test the tissue adhesion of the hydrogel.

Meanwhile, lap-shear test was performed on a universal testing machine (UTM2503, Shenzhen Suns Technology). Hydrogels were applied to dry porcine skins with a bonding area of 15 mm × 15 mm. Then lap-shear test was conducted to evaluate the adhesion force.

2.7. Self-healing test

Self-healing capability of the hydrogel was evaluated by three independent experiments. In the first test, a round hydrogel was cut into two pieces, the separate parts were brought into contact and placed at room temperature for 3 min for healing. Afterwards, external tension was applied to the healed hydrogel with tweezers. In the second test, hydrogel was cut into small pieces, then brought together with finger compression for 30 s. Then 10 mL air was injected into the healed hydrogel with a syringe, the hydrogel was monitored to assess its ability to withstand deformation. In the last test, a round shaped hydrogel was cut with a scalpel, punctured with a needle consecutively, the recovery of the hydrogel was observed afterwards.

2.8. Swelling of hydrogels

To evaluate the swelling characteristics, PAE hydrogels with identical weights were submerged in 15 mL of PBS solution (pH = 7.4) at 37 °C with an agitation of 100 rpm. At specific time intervals, the specimens were extracted and weighted after eliminating excess water with filter paper. The swelling ratio of the hydrogel was calculated using the following formula:

$$Swelling\ ratio = \frac{W_t}{W_0} \times 100\%$$

where W_t and W_0 represent the weight of the swollen hydrogel at different time points and the initial dry weight of the hydrogel, respectively.

2.9. Drug release profile

EGCG release from PAE hydrogels was first tested in PBS. Briefly, 1 g of PAE 3, PAE 5 and PAE 8 hydrogels were added into centrifuge tubes with 20 mL fresh PBS (0.01 M, pH 7.4), respectively. The tubes were kept at 37 °C with shaking of 100 rpm for different incubation times, including 1 h, 2 h, 4 h, 12 h, 1 d, 2 d, 3d, 4 d, 6 d, 8 d, 10 d, 14 d and 16 d. At each time point, 3 mL supernatants were extracted and compensated with 3 mL fresh PBS. The concentration of released EGCG was determined by measuring the absorbance at 276 nm using an UV–Vis–NIR Spectrophotometer (Cary 5000, Agilent). The accumulative release of EGCG from hydrogels was expressed as a percentage of the released drug and plotted over incubation time.

Similarly, the glucose-responsive releasing profile of PAE hydrogel was also tested. 1 g PAE 8 hydrogels were incubated in 20 mL PBS (0.01 M, pH 7.4) or in PBS with 25 mM glucose at 37 °C, respectively. The drug release profile upon glucose concentrations was measured and plotted similarly as the above description.

2.10. Hemolysis test

First, 100 mg PAE hydrogel was incubated in 10 mL PBS (0.01 M, pH 7.4) at 37 °C with agitation at 100 rpm for 24 h, the supernatant was collected and filtered by a 0.22 μm filter (Yeasen Biotechnology) to obtain sterile hydrogel extract. Fresh rat blood was collected, and centrifuged at 1500 rpm for 30 min to completely remove the serum. The obtained red blood cells (RBCs) were diluted by 0.01 M PBS to 16 % (v/v). The diluted RBCs were incubated with sterile hydrogel extract (1:1 (v/v)) at 37 °C for 1 h. PBS solution and Triton X-100 (1 %)-treated RBCs were used as negative and positive control, respectively. Afterwards, the suspension was collected and centrifuged at 1500 rpm for 10

min. The supernatant was collected, and the absorbance at 541 nm was measured by a microplate reader (VICTOR Nivo Multi Microplate Reader, PerkinElmer). And the hemolysis rate was calculated as below:

$$Hemolysis\ rate = \frac{A_t - A_n}{A_p - A_n} \times 100\%$$

where A_t, A_n and A_p are the absorbance of the hydrogel extract group, negative control group, and positive control group, respectively.

2.11. Cytocompatibility evaluation

L929 cells (Thermo Fisher Scientific) were cultured in DMEM medium (Thermo Fisher Scientific) supplemented with 10 % fetal bovine serum (FBS) and 1 % penicillin-streptomycin in a 5 % CO_2 incubator at 37 °C. 100 mg PAE 8 hydrogel was incubated with 10 mL cell culture medium for 24 h at 37 °C, the PAE hydrogel extract was obtained after filtration. L929 cells were seeded in 96-well plate at a density of 2000 cells/well, and adhered to the plate for 12 h, then the culture medium was replaced with 100 μL PAE hydrogel extract. The cell culture medium served as control. The medium was refreshed every 24 h. After 24 h or 48 h incubation, cell viability was evaluated using CCK-8 kit (Beyotime Biotechnology). 10 μL CCK-8 solution was added to each well and incubated for 2 h. The absorbance at 450 nm was recorded using the VICTOR Nivo Multi Microplate Reader. The relative cell viability was expressed as:

$$Cell\ viability = \frac{A_t}{A_c} \times 100\%$$

where A_t and A_c represent the absorbance of the test sample and the control group, respectively.

Meanwhile, live/dead staining was conducted with L929 cells. The cells were planted into a 6-well plate with a density of 8×10^4 cells/well and cultured in cell culture medium for 12 h, before it was replaced with PAE hydrogel extract. Cells cultured with cell culture medium serves as control. After further culture for 24 or 48 h, cells were stained with 1 mL of calcein-AM and propidium iodide dye (Beyotime Biotechnology) for 30 min, which stained viable cells and dead cells, respectively. Cells were then observed under an inverted fluorescence microscope (IX73, Olympus) for green and red fluorescence. All experiments were performed in triplicate.

2.12. Antioxidant efficiency evaluation

The antioxidant efficiency of hydrogels was evaluated by 2,2-Diphenyl-1-picrylhydrazyl (DPPH) free radical scavenging assay and reactive oxygen species (ROS) assay, respectively. In first assay, scavenging of the DPPH free radical by PAE hydrogel was evaluated. The hydrogels were homogenized using a tissue grinder. Then 100 μM DPPH (Beyotime Biotechnology) and different amounts of hydrogels (3 mg, 9 mg, 15 mg, and 30 mg, respectively) were dispersed in 3.0 mL ethanol. After agitation and incubation in dark at 37 °C for 30 min, 200 μL supernatant was collected, and the optical density at 517 nm were measured. The degradation of DPPH was calculated by the following formula:

$$Scavenging\ rate = \frac{A_{Blk} - A_{Hydrogel}}{A_{Blk}} \times 100\%$$

where A_{Blk} and $A_{Hydrogel}$ are the absorbance of the blank group (DPPH) and the hydrogel group (DPPH + PAE hydrogel), respectively.

Next, the intracellular ROS scavenging ability of hydrogel was measured using ROS assay kit (Thermo Fisher Scientific). L929 cells (1×10^6 cells/well) were seeded in a 6-well plate and incubated for 12 h. Cells were first treated with 1 mL dichlorofluorescein diacetate (DCFDA, 0.01 mM) in serum-free medium and incubated for 30 min, then disposed with DMEM solutions containing 10 mg/mL PAE 8 hydrogel and Rosup (0.05 mg/mL) for 30 min. Cells with only Rosup treatment were used as the positive control, and cells with no treatment were used as negative control. Subsequently, the cells were imaged by an inverted fluorescence microscopy (IX73, Olympus) with random fields using the same exposure parameter. Meanwhile, the fluorescence intensity of the above treated cells was measured by flowcytometry (Cytoflex S, Beckman).

2.13. Tube formation assay

Tube formation assay was performed to evaluate the angiogenic potential of PAE hydrogels. First, sterilized PAE 8 hydrogels were incubated with cell culture medium for 24 h to obtain fresh PAE 8 hydrogel extract. 200 μL of Matrigel (Corning) was added to a 48-well plate, followed by gel at 37 °C for 30 min. Then, human umbilical vein endothelial cells (HUVECs) at a density of 3×10^4 cells per well were seeded onto the Matrigel, and incubated in 200 μL of media, including different hydrogel extract (1 mM, 5 mM, and 10 mM) and PBS as control group. After 6 h incubation, the formation of capillary-like structures was imaged under an inverted microscope (IX73, Olympus). Quantitative analysis of the tube networks was conducted using angiogenesis analyzer in ImageJ software (NIH), including the number of junctions, number of nodes, and the total segment length [32].

2.14. Antibacterial activity evaluation

Staphylococcus aureus (*S. aureus*) and *Escherichia coli* (*E. coli*) were incubated in a Luria-Bertani (LB) broth at 37 °C overnight. Meanwhile, PAE hydrogels were washed in 75 % ethanol and PBS for 3 times for sterilization. 500 mg sterilized PAE hydrogels were then added to a 10 mL centrifuge tube, while 500 μL of PBS was used as the control. Next, 3 mL of diluted bacterial suspension in PBS (1×10^4 CFU/mL) were added to each tube. The tubes were then incubated in a humidified incubator at 37 °C under agitation for 24 h. To determine the number of living bacteria in each tube, 100 μL of the supernatant from each tube was transferred into a 96-well plate, and 10 μL of CCK-8 solution was added. After incubation for 1 h, the absorbance was measured at 450 nm using the VICTOR Nivo Multi Microplate Reader. The killing ratio of bacteria was calculated using the following equation:

$$Killing\ ratio = \frac{A_c - A_t}{A_c} \times 100\%$$

where A_t and A_c represent the absorbance of the test sample and the control group, respectively.

Additionally, 100 μL of the supernatant from each tube was spread onto the LB agar plates. Then the plates were incubated for 24 h, and the growth of bacteria was photographed by high resolution camera.

2.15. Anti-inflammation test

To investigate the anti-inflammation property of PAE hydrogel, a high glucose-induced inflammatory cellular model was established. According to our previous protocol [33], human umbilical vein endothelial cells (HUVECs, Thermo Fisher Scientific) were incubated with cell culture medium with supplementary of 5 mM glucose (low glucose, LG), 25 mM glucose (high glucose, HG) or 25 mM glucose plus 10 mg/mL hydrogel extract (HG + PAE). After 3 days, the cells were harvested, and the levels of interlukin-1β (IL-1β) and interlukin-6 (IL-6) in the cells were evaluated using the human IL-1β ELISA kit (Servicebio) and human IL-6 ELISA kit (Servicebio) according to the manufacturer's instructions, respectively.

2.16. Diabetic wound healing test

All animal studies in this study were performed in accordance with

the guidelines approved by the Institutional Animal Care and Use Committee of Wuhan University (IACUC Number: WP20230364). Male SD rats (200–250 g) were acclimatized for 5 days. After an 8-h fasting, the rats received intraperitoneal injection of streptozotocin (STZ) at a dose of 75 mg/kg, this procedure was performed every day for 3 consecutive days. After that, the blood glucose levels of rats were continuously monitored every 3 days for 2 weeks, and the rats with stable glucose level of >16.6 mM were considered as successful type I diabetic model. Afterwards, the animals were randomly divided for further experiments.

Animals were anesthetized by sevoflurane inhalation, and the dorsal of rats were shaved or depilated. A circular biopsy punch with a diameter of 12 mm was used to induce full-thickness wounds on the dorsal of rats. Diabetic wounds were received different treatments, including AA-Am hydrogel, PAE hydrogel, E-F solution with same level of EGCG in PAE hydrogel, DuoDERM® wound dressing (Convatec), or left untreated as negative control. All wound dressings were changed every 7 days, for the E-F group, same amount of solution was sprayed. Wounds were photographed at different time points during healing process, and wound areas in each group were measured by ImageJ software (NIH).

2.17. Histological analysis

At day 10 and day 19 post-injury, skin tissues surrounding the wounds were collected and fixed for histological analysis. Skin tissues were sectioned, and stained with hematoxylin & eosin (H&E) and Masson's trichrome staining kits, the slices were visualized with Case-viewer software (3DHISTECH).

In addition, skin tissues on day 19 were examined using immunofluorescence staining. Skin tissue slices were incubated with primary antibody, including rabbit polyclonal antibody against CD 31 (Abcam, 1:100), rabbit polyclonal antibody against TNF-α (Abcam, 1:200), rabbit monoclonal antibody against F4/80 (Abcam, 1:100), and goat monoclonal antibody against CD 163 (Abcam, 1:200), respectively. Afterwards, the secondary antibody corresponding to the primary antibody with different fluorescence were bounded, where CD 31 and CD 163 was stained in red fluorescence, while TNF-α and F4/80 was stained in green fluorescence. Cell nuclei were stained with 4′,6-diamidino-2-phenylindole (DAPI, Abcam) with blue fluorescence. The slices were protected with antifade reagent, observed with fluorescence microscopy (Aperio Versa 8, Leica), and quantitatively analyzed by ImageJ software.

2.18. Statistical analysis

At least three independents were included for each experiment. Data were presented by mean ± SD. Statistical analysis was performed using one-way analysis of variance (ANOVA) for multiple groups. P values were noted as *p < 0.05, **p < 0.01, ***p < 0.001, ****p < 0.0001. And

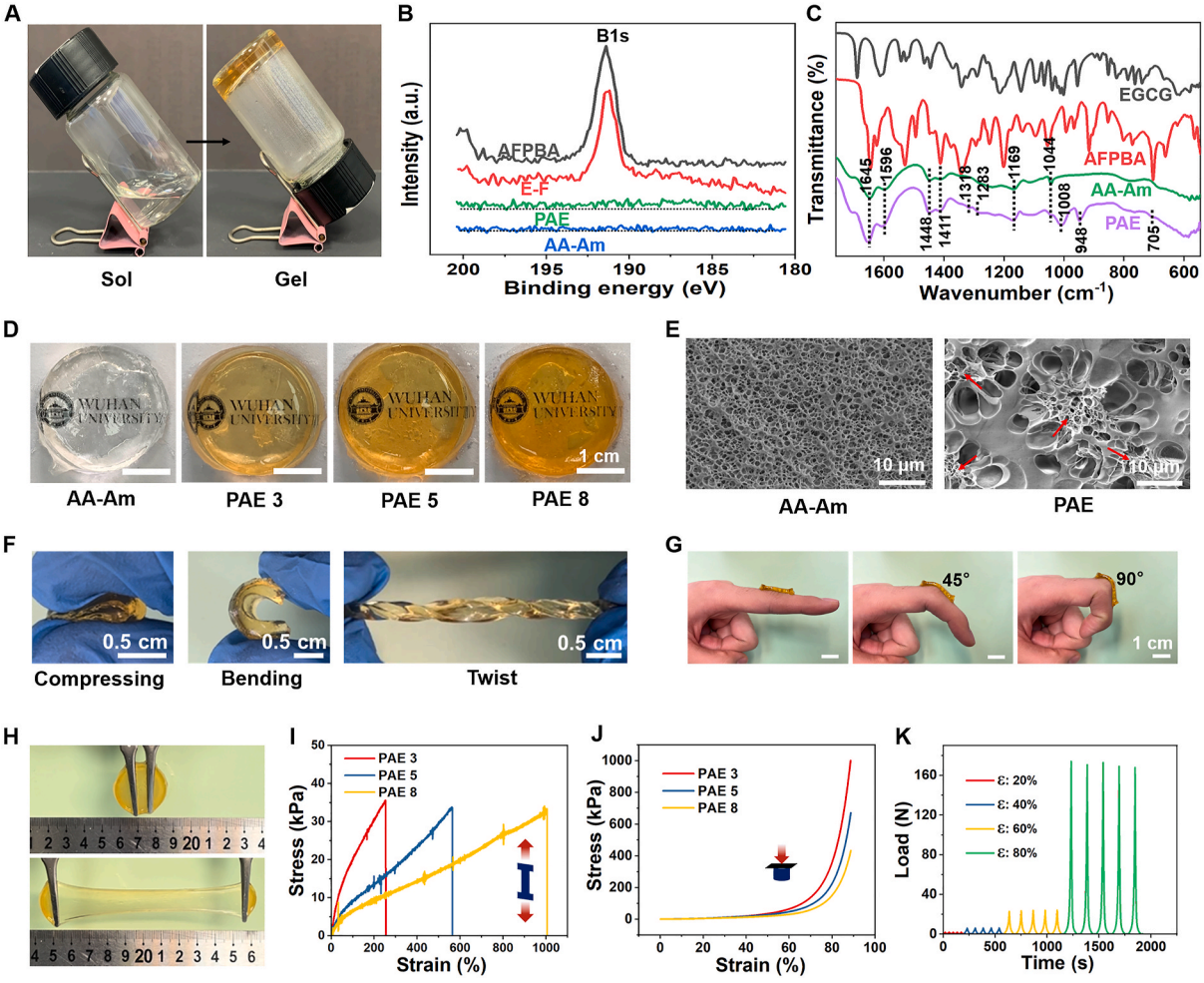

Fig. 2. Physicochemical characterization of PAE hydrogels. (A) Sol-gel transformation of PAE hydrogel. (B) XPS high-resolution spectra of B1s during the synthesis of PAE hydrogel. (C) FTIR spectra during the synthesis of PAE hydrogel. (D) Morphology and transparency of AA-Am and PAE hydrogels. (E) SEM images of AA-Am and PAE 8 hydrogel. Red arrows indicate the crosslinked areas in the hydrogel network. (F) Deformability of PAE hydrogels. (G) Adhesion and bending of PAE hydrogel on finger joint. (H) PAE hydrogel before and after large stretching by external force. (I) Tensile stress-strain curves of PAE hydrogels. (J) Compressive stress-strain curves of PAE hydrogels. (K) Cyclic compressive test of PAE 8 hydrogel with different strain.

P value of <0.05 is regarded as statistically significant, ns as not significant ($p > 0.05$).

3. Results and discussion

3.1. Synthesis and characterization of PAE hydrogels

PAE hydrogel was synthesized through the radical polymerization between AA-Am precursor solution and dynamic E-F crosslinker (Fig. 1A–C). E-F crosslinker was formed based on the reversible binding of phenylboronic acid of AFPBA molecule with the diol group of EGCG, which formed a cyclic boronate (Fig. 1A) [34–36]. During the photopolymerization of AA-Am (Fig. 1B), the addition of E-F crosslinker, which served as the second network, enhanced the molecular chain connection of AA-Am, via radical polymerization as well as hydrogen bonding (Fig. 1C). The mixture of AA-Am precursor solution and E-F crosslinker (1–11 mM) presented a sol state at room temperature (Fig. 2A), and the mixture underwent sol-gel transition after about 10 min of polymerization in 60 °C (Table S1). PAE hydrogel with 1 mM E-F crosslinker showed similar sol-gel transition process as AA-Am hydrogel, which showed a gelation time of 8.5 ± 1.3 min (Table S1). With the addition of more E-F crosslinker (3–8 mM), the time for sol-gel transformation was increased from 9.6 ± 0.3 to 15.7 ± 2.4 min (Table S1). PAE hydrogel with higher concentration of E-F crosslinker (11 mM) was hard to form hydrogel, due to the excess catechol groups from EGCG (Fig. 1A), which interfered the free radical polymerization process [37]. Therefore, PAE hydrogels with 3, 5 and 8 mM E-F crosslinker were selected for further experiments.

The successful synthesis of PAE hydrogel was evaluated by X-ray photoelectron spectroscopy (XPS) and Fourier transform infrared (FTIR) spectroscopy. We first analyzed the changes of atomic composition during the synthesis of PAE hydrogel with XPS. Compared to AFPBA which contained substantial B and F (Fig. S1, Table S2), E-F crosslinker showed decreased B and F content (Fig. S1, Fig. 2B–Table S2). After further crosslinking of AA-Am with E-F crosslinker, the obtained PAE hydrogel demonstrated the existence of surface B and F due to the presence of AFPBA molecule in the hydrogel (Fig. 2B, Fig. S1B), with a decreased ratio of B and F to 0.72 % and 1.25 %, respectively (Table S2). These results suggested the successful integration of AFPBA as well as E-F crosslinker into PAE hydrogel.

The chemical structure during the synthesis of PAE hydrogels was further evaluated using FTIR. In general, the FTIR spectrum of PAE hydrogel approached to that of AA-Am hydrogel (Fig. S2, Fig. 2C), including the absorption peaks at 3346 cm^{-1} and 3197 cm^{-1} due to the asymmetric and symmetric $–NH_2$ stretching (Fig. S2A), the $–CH_2$ stretching vibrations at 2933 cm^{-1} (Fig. S2A), the peak of O–H of carboxylic acid at 1700 cm^{-1} (Fig. S2A) [38], and C═O stretching vibration at 1645 cm^{-1} and 1448 cm^{-1} (Fig. 2C), the bonding and bending vibration of N–H at 1596 cm^{-1} and 1411 cm^{-1}, C–O and C–O–C stretching at 1169 cm^{-1} and 1044 cm^{-1} (Fig. 2C) [38]. The similar FTIR spectra between AA-Am and PAE hydrogel was due to the main content of AA-Am (20:1) in PAE hydrogel (Fig. 1A–C). Besides, EGCG and AFPBA exhibited bond characteristics with abundant functional groups (Fig. S2). For PAE hydrogel, the FTIR spectrum was similar to AA-Am, however, with existence of additional characteristic peaks originated from EGCG (such as at 1318 cm^{-1}, 1283 cm^{-1}, 1008 cm^{-1}, and 948 cm^{-1}) and AFPBA (such as at 705 cm^{-1}) (Fig. 2C, Fig. S2B), suggesting the efficient formation of crosslinked PAE hydrogel, with AA-Am as a backbone network, and E-F crosslinker as a secondary network.

After polymerization with E-F crosslinker, PAE hydrogel showed improved formability compared to AA-Am hydrogel, which made it much easier to be completely demolded without deformation or self-adhesion (Fig. S3). With the addition of E-F crosslinker, hydrogels changed from transparent to brown, and the color of PAE hydrogels became darker as the concentration of E-F crosslinker increased (Fig. 2D). Nevertheless, all PAE hydrogels were transparent enough to observe the letters below (Fig. 2D), which enables future wound observation with application as hydrogel dressing. Meanwhile, microscopic morphology features of hydrogels were characterized by SEM. Compared to AA-Am hydrogel with small, uniformly distributed pores ranged of 1–5 μm, PAE hydrogels exhibited larger and clustered pores, with pore sizes up to 10 μm (Fig. 2E, Fig. S4). This phenomenon could be attributed to the dynamic crosslinking effect of E-F crosslinker, which contracted the surrounding network through intermolecular interaction [23].

3.2. Mechanical property of PAE hydrogels

For wound treatment, the overall strength of wound dressing is critical during their practical application against normal body movement and potential stress such as compression, puncturing, and slicing. Ideal wound dressing should possess adequate recoverability and withstand the intense activity as well as frequent movement during the wound healing process. The mechanical properties of PAE hydrogels were systematically evaluated. First, we studied the overall strength of PAE hydrogel macroscopically. The hydrogel (PAE 8 as an example) was strong enough to withstand multiple mechanical tests such as compressing, bending and twisting (Fig. 2F). Moreover, PAE hydrogels showed excellent flexibility, and could firmly attach to human finger joint with different degree of bending (Fig. 2G). In Fig. 2H–a round hydrogel was stretched 10 times to its initial length by external force, presenting great tensile property.

The mechanical properties of PAE hydrogels were further quantitatively evaluated by tensile and compressive tests. As the concentration of E-F crosslinker increased, the tensile strength of PAE hydrogels slightly decreased (Fig. 2I). PAE 8 hydrogel showed a maximum elongation of 1005.8 % and a tensile strength of 33.2 kPa (Fig. 2I), which is enough for wound dressing. Compared to pure AA-Am hydrogels with an elongation of 380 % and a tensile strength of 70 kPa (Table S3) [18], PAE hydrogels exhibited an obvious yield-softening progress, the tensile strength decreased to 25.8 ± 4.4 kPa (Fig. S5A), while the elongation at break increased to 906.5 % ± 75.5 % for PAE 8 hydrogel (Fig. S5B), which was about 2.4 folds of pure AA-Am hydrogels. In the compression tests, PAE hydrogels in all three groups could withstand compressive strain to over 85 %, while the tensile compressive stress decreased as the E-F crosslinker concentration raised (Fig. 2J). Furthermore, PAE hydrogel demonstrated the ability to recover to its initial condition when subjected to successive stepwise compression (Fig. S6), also maintained its mechanical strength after 5 cycles with stepwise increased load (Fig. 2K). Overall, PAE hydrogels exhibited good flexibility and durability to resist external force. Their ability to adhere to human skin and joints, coupled with their exceptional mechanical property, made them well suitable for use in wound dressing applications.

3.3. Tissue adhesion performances of PAE hydrogels

Strong wet tissue adhesion of hydrogels is important during the application as wound dressing [39,40]. Multiple tests were carried out to evaluate the adhesiveness of PAE hydrogels. PAE hydrogels could easily adhere to human skin, and no residue left on the skin after being peeled off (Fig. 3A). Moreover, the hydrogel showed good adherence to multiple substrates including rubber gloves, metal, glass, polypropylene, wood and polyethylene (Fig. S7). Push-out test was carried out to investigate the tissue adhesion ability. PAE hydrogel firmly adhered to porcine tissues including muscle, kidney, liver and skin (Fig. 3B, Fig. S8). In the lap-shear test, the adhesion strength of PAE hydrogels increased as the concentration of E-F crosslinker increased (Fig. 3C), with 1.5 ± 0.5 kPa for PAE 3 hydrogel and 5.6 ± 1.2 kPa for PAE 8 hydrogel. To assess the safety of use, we compared the peeling damage to rat skin tissues between PAE hydrogel and medical adhesive fabric tape. There was visible subcutaneous hemorrhage immediately after the peeling of tape, and a rupture of epidermis was observed in H&E staining

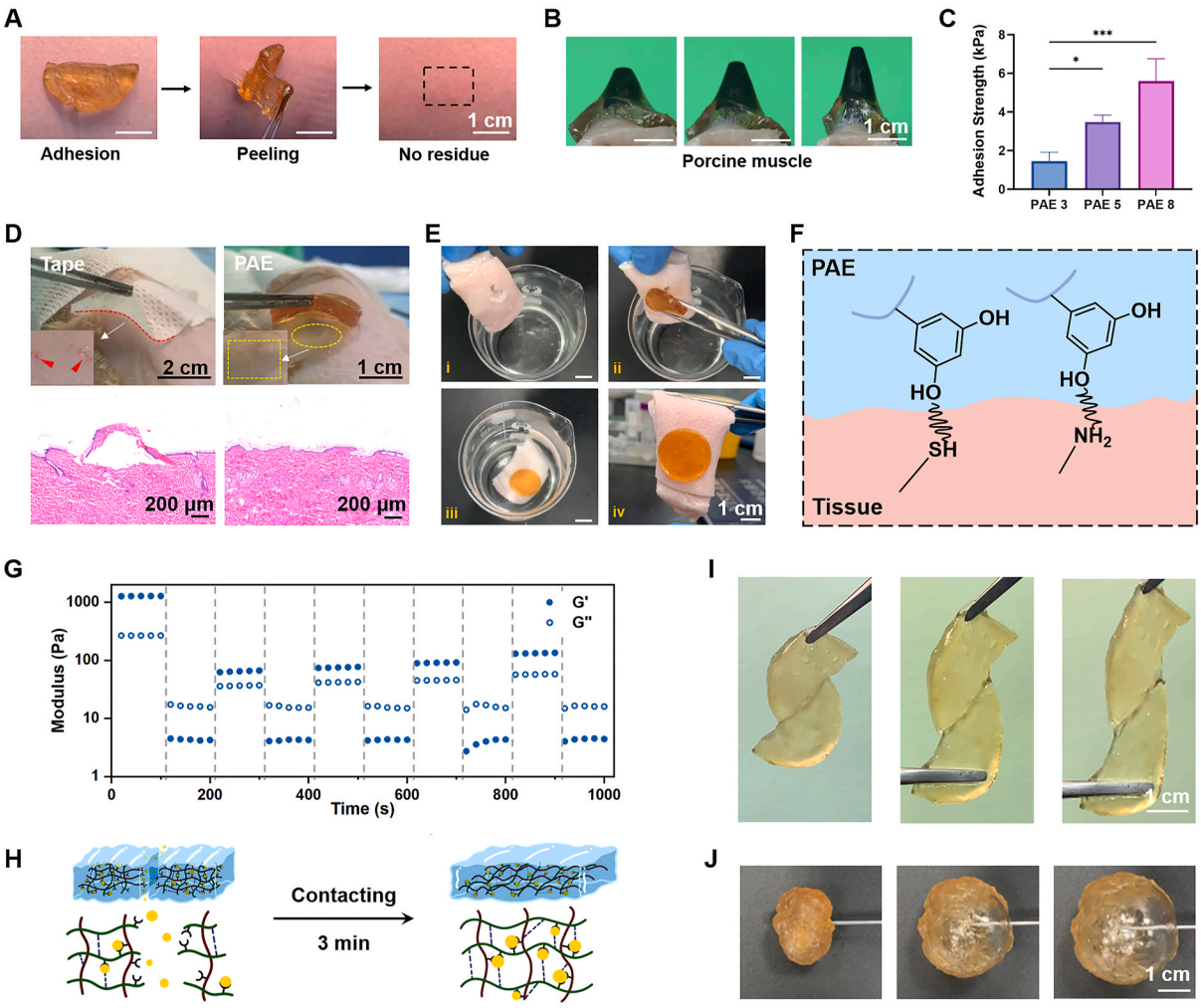

Fig. 3. Tissue adhesion and self-healing properties of PAE hydrogels. (A) Adhesion and peeling of PAE hydrogel on arm. No residue left after peeling off the hydrogel. (B) Images of strong adhesion and stretch ability of PAE hydrogel on porcine muscle. (C) Adhesion strength of PAE hydrogels on porcine skin. (D) Comparison of peeling damages on rat skin induced by medical adhesive fabric tape and PAE hydrogel, respectively. Red marks show the subcutaneous hemorrhage caused by peeling damage. Yellow dotted rectangle and circle show the peeled area of PAE hydrogel. (E) Representative images of wet adhesion of PAE hydrogel on porcine skin. (F) Illustration of adhesion mechanism of PAE hydrogels on tissues. (G) Step-strain sweeps to confirm self-healing capacity of PAE hydrogel. (H) Self-healing mechanism of PAE hydrogel, including bond rearrangements of boronic esters and hydrogen bonding. (I) Stretching of healed PAE hydrogel by external force. (J) Inflation of healed PAE hydrogel with 10 mL air injection.

(Fig. 3D). In contrast, there was no apparent change of skin in post-peeling stage or H&E staining for PAE hydrogel group (Fig. 3D), indicating its excellent safety in comparison to conventional medical wound dressing.

Considering the moist environment caused by excessive exudate in diabetic wounds, wet adhesion is critical for hydrogel wound dressing. Ideal wound dressing should firmly adhere to wet wound surface, and remove the excessive exudate from the wound site [41,42]. The wet adhesion behavior of PAE hydrogel was evaluated. PAE hydrogel was applied on the wound of a wet porcine skin (Fig. 3$E_{i\text{-}ii}$), and then immersed into water for 20 s (Fig. 3E_{iii}). PAE hydrogel remained firmly attached to the wound site after taking out from underwater (Fig. 3E_{iv}), representing its strong wet surface adhesion and endurance even underwater. The bonding between phenolic hydroxyl groups in PAE hydrogel and amino groups, thiol groups in tissues contributed to the strong adhesiveness (Fig. 3F).

Besides of wet adhesion ability, interestingly, we found that PAE hydrogels absorb considerable amount of liquid when immersed in PBS solution. PAE hydrogel was attached on the surface of a piece of cardboard, and soaked into water (Fig. S9), mimicking the wet environment of diabetic wounds. After 48 h, PAE hydrogel absorbed considerable amount of liquid. However, PAE hydrogel still firmly adhered to the cardboard surface after 48 h underwater, which ruptured under shear force rather than de-adhesion (Fig. S9).

3.4. Self-healing properties of PAE hydrogels

Besides of strong adhesion ability in dry and wet environment, the dynamic and self-healing of PAE hydrogels were investigated. In rheological analysis, strain amplitude sweep tests were applied to determine the critical strain for disrupting the network of PAE 8 hydrogel, and the critical strain was found to be 763.3 % (Fig. S10). Hydrogel with self-healing ability could greatly maintain the stability when subjected to external mechanical forces. Next, the self-healing properties of hydrogel were quantitatively examined by using step-strain measurements. Based on the above critical strain point, 1200 % was selected as large strain, and small strain was fixed at 1 %. For PAE 8 hydrogel, G′ was higher than G″ when under small strain of 1 % (Fig. 3G). As the strain was switched to 1200 %, G″ was higher than G′ (Fig. 3G), indicating the disruption of the hydrogel network. When small strain processed again, G′ and G″ recovered (Fig. 3G), revealing the network of PAE 8 hydrogel restored during five cycles of oscillation strain.

Subsequently, the self-healing ability of PAE hydrogel was also macroscopically evaluated. After being cut and punctured consecutively, PAE hydrogel quickly healed within few seconds (Fig. S11A). PAE hydrogel were cut into two parts, then staggered and contacted for self-healing. PAE hydrogel exhibited fast healing within 3 min at the interfaces of damage (Fig. 3H), the healed hydrogel not only could resist gravity, but also withstand stretching force along the healing line (Fig. 3I). Moreover, after being split into pieces and immediately reassembled for 30 s (Fig. S11B), the healed hydrogel could withstand as much as 10 mL air inflation (Fig. 3J, Movie S1). When the PAE hydrogel was disrupted by an external force, the boronate esters in its structure disassembled (Fig. 3H, left), however, they promptly reorganized themselves as soon as the separated surfaces came into contact, the re-establishment of hydrogen bonds also accelerated this process (Fig. 3H, right) [42], which together resulted in an immediate self-healing response. These findings suggest that PAE hydrogel possesses rapid self-healing characteristics.

3.5. Swelling and drug release profile of PAE hydrogels

Hydrogels generally swell when exposed to solutions. When immersed in PBS, all PAE hydrogels swelled rapidly within 24 h, and reached equilibrium in 2 days (Fig. 4A–B). With lower concentration of E-F crosslinker (PAE 3 and PAE 5), the maximum swelling was 625.6 % ± 45.4 % and 653.4 % ± 29.2 %, while the PAE hydrogel with 8 mM E-F crosslinker showed highest water absorption with a maximum swelling of 1006.5 % ± 35.6 % (Fig. 4B). This could be attributed to the three-dimensional network structure of PAE and the existence of abundant hydroxyl groups in EGCG. The larger swelling of PAE 8 hydrogel is potentially efficient for the absorption and elimination of diabetic wound exudate.

Along with the swelling of hydrogel, the inner structure of PAE hydrogel gradually broke down to release the therapeutic component of EGCG. The drug release profile of PAE hydrogels was first evaluated in PBS. PAE 3 hydrogel released 92.5 % ± 6.4 % of EGCG in the first 3 days and finished releasing in 6 days (Fig. 4C), while PAE 5 and PAE 8 hydrogel showed a slower releasing profile, and achieved maximum release at 14 days and 16 days, respectively (Fig. 4C). The lower concentration of E-F crosslinker (PAE 3) led to a faster release rate, due to the less crosslinking density of the hydrogel networks. It should be note that the release of EGCG from PAE hydrogel could lead to a weaken tissue adhesion, facilitating the removal of PAE hydrogel dressing after use.

Considering the dynamic bonding between EGCG and AFPBA, the PAE hydrogel are responsive to polyhydroxy compounds such as glucose [30]. To investigate the glucose-responsive releasing property of PAE hydrogels, the drug release from PAE 8 hydrogels in PBS and high glucose solution (HG) was investigated. Comparably, the release of EGCG from PAE hydrogel was much faster in HG solution than that in PBS (Fig. 4D). The above results indicate that PAE hydrogels are effective at absorbing substantial amounts of exudate, and exhibited high glucose-responsive drug release, making it good potential for use in diabetic wound dressing.

3.6. In vitro biocompatibility of PAE hydrogels

Cell compatibility of PAE hydrogel was evaluated by CCK-8 assay and live/dead staining using L929 cells. In live/dead staining, live and dead cells were stained with green and red fluorescence, respectively. Cells in both PAE hydrogel extract and control group showed similar proliferation and similar morphology after incubation for 24 h and 48 h (Fig. 5A). Afterwards, CCK-8 assay was performed to evaluate the viability of cells treated with different concentration of hydrogel extract. As the concentration of PAE hydrogel extract reached 10 mg/mL, cell viability was still higher than 95 % after 24 h or 48 h incubation (Fig. 5B). Moreover, no obvious difference was found between control group and hydrogel groups, indicating good cell compatibility of PAE hydrogels.

To further investigate the blood compatibility of PAE hydrogels, rat RBCs were used for hemolysis test. Compared to positive control group, no visible hemolysis was observed for PBS-treated and hydrogel-treated RBCs (Fig. S12), and no significant hemolytic activity was observed in

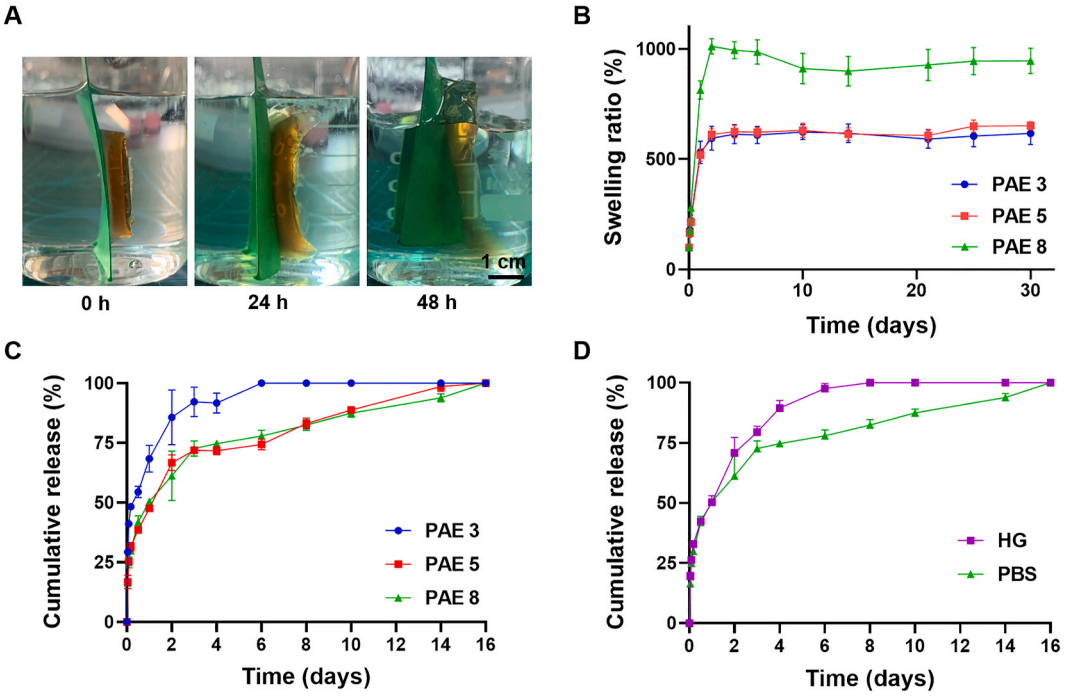

Fig. 4. Swelling property and drug release profile of PAE hydrogels. (A) Photos of PAE 8 hydrogel before and after swelling in PBS for 24 h and 48 h. (B) Mass swelling ratio of PAE hydrogels immersed in PBS at 37 °C for 30 days. (C) Cumulative release of EGCG from PAE hydrogels. (D) Cumulative release of EGCG from PAE 8 hydrogel immersed in PBS and in high glucose concentration (HG), respectively.

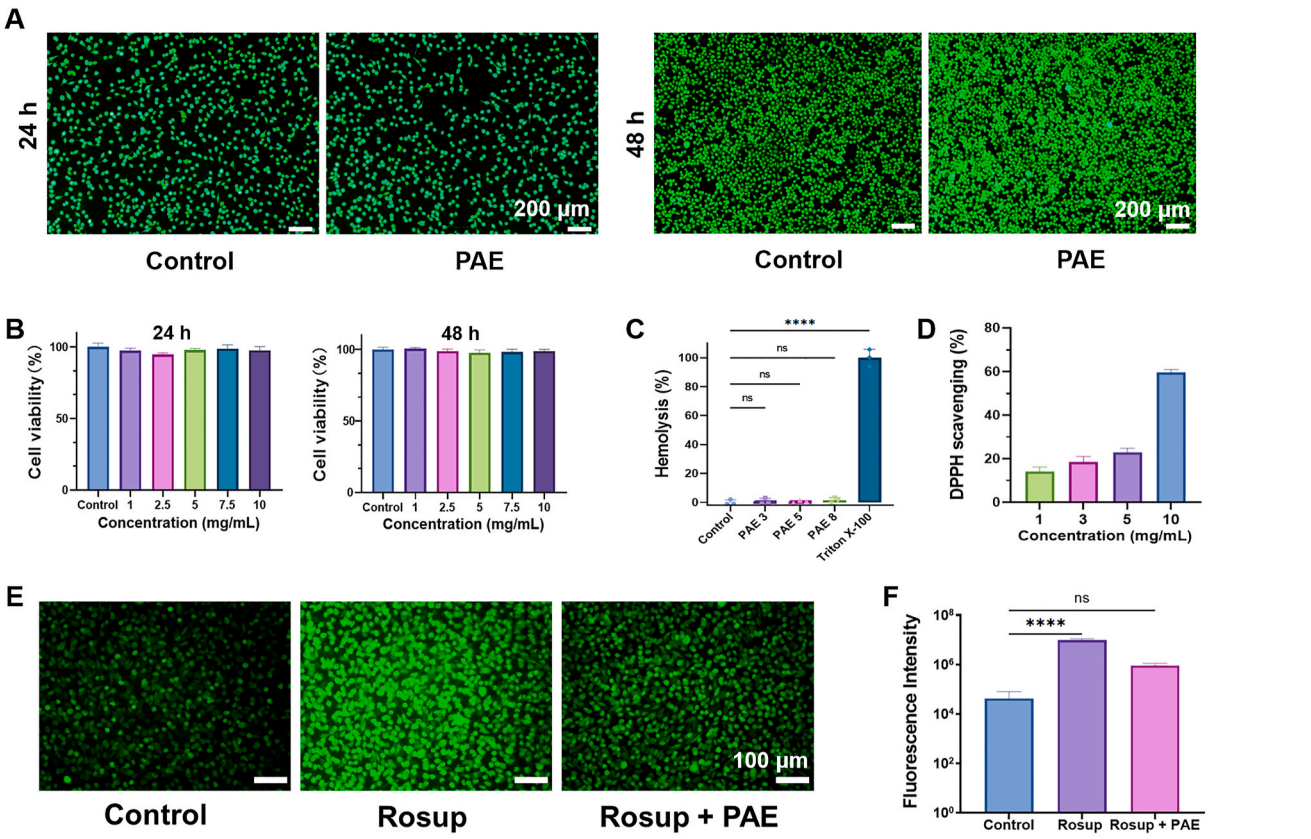

Fig. 5. Biocompatibility and antioxidative activities of PAE hydrogels. (A) Live/dead staining of L929 cells after treated with PAE 8 hydrogel for 24 h and 48 h. (B) Cell viability of L929 cells treated with different concentrations of PAE 8 hydrogels for 24 h and 48 h. (C) Hemolysis rate after treatment with PAE hydrogels. (D) DPPH scavenging capability of PAE 8 hydrogels. (E) Intracellular ROS scavenging ability of PAE hydrogels by DCFDA staining. (F) Fluorescence intensity of DCFDA staining. Data are shown as mean ± SD, n = 3. ****p < 0.0001, ns means non-significant (p > 0.05).

the PAE treatment groups (Fig. 5C). Therefore, PAE hydrogels showed good biocompatibility, suggesting their safety for utilization as wound dressings.

3.7. In vitro antioxidant effect

In diabetic wounds, the excessive generation of reactive oxygen species (ROS) is one of the major reasons for delayed healing [43]. We first investigated the antioxidant effect of PAE hydrogel by measuring DPPH free radicals scavenging activity. The DPPH scavenging ability of PAE hydrogels showed a concentration-dependent manner (Fig. 5D). When the concentration of PAE hydrogel reached 10 mg/mL, the DPPH scavenging rate raised to about 60 % compared to 22 % of 5 mg/mL PAE hydrogel (Fig. 5D).

To further test the intracellular ROS scavenging ability of PAE hydrogels, L929 cells were incubated with DMEM solutions containing 10 mg/mL PAE hydrogels with Rosup agent, which stimulate the cell to produce excessive ROS intracellularly. Dichlorofluorescein diacetate (DCFDA) was used as a probe to detect the intracellular ROS level. Fluorescence level of DCFDA was much higher in Rosup group compared to control group (Fig. 5E), indicating an excessive intracellular ROS production. This phenomenon was reversed by the incorporation of PAE hydrogel (Fig. 5E), demonstrating its good intracellular ROS scavenging capacity. Moreover, the mean fluorescence intensity level of DCFDA in cells was quantified by flowcytometry (Fig. 5F). Significant difference of fluorescence intensity between control group and Rosup group was detected, while there was no difference between PAE hydrogel and control group (Fig. 5F). These results suggested that PAE hydrogel possess potent ROS scavenging ability in both intracellular and extracellular conditions.

3.8. In vitro angiogenesis activity

Promoting angiogenesis was advantageous to modulate the wound microenvironment and accelerate diabetic wound healing [32]. Tube-formation assay was used to evaluate the effect of PAE hydrogels on angiogenesis. Compared to the PBS control group, the angiogenesis capacity was significantly enhanced by PAE hydrogel extract (Fig. 6A). With increased concentration of PAE hydrogel extract from 1 mM to 10 mM, the pro-angiogenesis activity of PAE hydrogels became more significant (Fig. 6A). The concentration of 10 mM PAE hydrogel extract exhibited the most significant stimulatory effects on tube formation, which exhibited most junctions, most nodes, and longest tubular length (Fig. 6B). These results demonstrated that PAE hydrogels exhibited significant angiogenesis activity.

3.9. Antibacterial effect

Persistent bacterial infection often occurs in diabetic wounds [44]. Hence, wound dressings with robust antibacterial capability hold substantial potential for practical clinical usage [45–47]. To evaluate the antibacterial activities of PAE hydrogels, Gram-positive bacterium of *S. aureus* and Gram-negative bacterium of *E. coli* were cultured with PBS or PAE hydrogels at 37 °C for 24 h. After incubation, bacterial suspension treated with PAE hydrogels were clear (Fig. S13), whereas the suspension treated with PBS control was cloudy due to the proliferation of bacteria (Fig. S13). Subsequently, the supernatant in each group was spread onto the LB agar plates, and the bacteria were incubated for 24 h. As a result, there were much fewer colony-forming units (CFUs) in PAE hydrogel groups compared to control group, which was almost fully covered by bacterial colonies (Fig. 6C). Notably, when the concentration

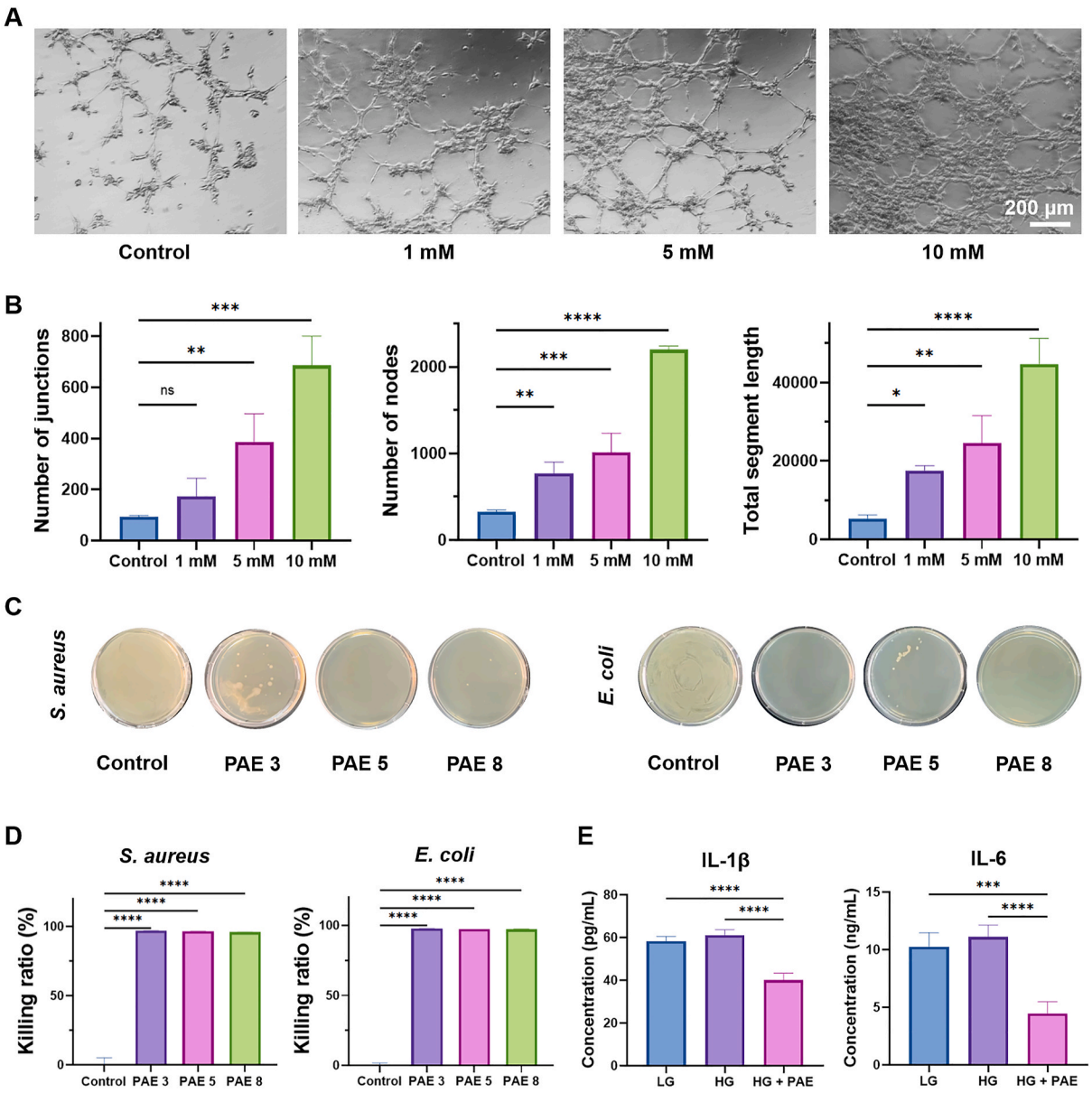

Fig. 6. *In vitro* angiogenesis capacity, antibacterial and anti-inflammation activities of PAE hydrogels. (A) Optical images of tube formation by HUVECs treated with different concentrations of PAE 8 hydrogel. (B) Quantification of angiogenesis through counting the number of junctions, the number of nodes and the total tubular length in each group. (C) Images of bacterial colonies of *S. aureus* and *E. coli* after cultured with PBS and PAE hydrogels. (D) Killing ratio of PAE hydrogels against *S. aureus* and *E. coli*. (E) Anti-inflammation activities of PAE hydrogel by reducing IL-1β and IL-6 levels in HUVECs. The cells were pre-treated with 5 mM glucose (LG), 25 mM glucose (HG), or 25 mM glucose plus 10 mg/mL PAE 8 hydrogel (HG + PAE). Data are shown as mean ± SD, n = 3. ***p < 0.001, ****p < 0.0001, ns means non-significant (p > 0.05).

of EGCG increased to 8 mM (PAE 8), CFUs were almost negligible in both *S. aureus* and *E. coli* groups (Fig. 6C), indicating the optimal concentration of EGCG should be no less than 8 mM in terms of antimicrobial effect. Moreover, the killing ratio of PAE 3, PAE 5 and PAE 8 hydrogels were 96.9 %, 96.4 % and 95.9 % in terms of *S. aureus*, respectively, and their killing ratio were 97.7 %, 97.4 % and 97.1 % for *E. coli*, respectively (Fig. 6D). Therefore, PAE hydrogel showed excellent antibacterial properties for both Gram-positive and Gram-negative bacterium.

3.10. Anti-inflammation activity

Diabetes-induced hyperglycemia leads to an aberrant release of inflammatory cytokines, including IL-1β and IL-6. These cytokines further aggravate inflammation at the wound site and impede the healing process [33]. To investigate the anti-inflammation effect of PAE hydrogels *in vitro*, HUVECs were incubated with glucose and PAE hydrogel extract, and the released IL-1β and IL-6 levels from cells were evaluated with ELISA. Elevated glucose levels had a modest impact on the release of inflammatory cytokines of IL-1β and IL-6 (Fig. 6E). However, under incubation with supplementary PAE hydrogel extract, the levels of IL-1β and IL-6 released by cells significantly decreased as compared to the low glucose (LG) or high glucose (HG) groups (Fig. 6E). These results suggested the efficient anti-inflammatory effect of PAE hydrogel even under high glucose condition, thus enhancing its usability in diabetic wound treatments.

3.11. Diabetic wound healing performance of PAE hydrogels

Besides of the therapeutic effect of PAE hydrogels *in vitro*, we further investigated the pro-healing properties of PAE hydrogel *in vivo* using a

full-thickness wound model in diabetic rats. The diabetic wounds were treated with different groups, including AA-Am hydrogel, E-F solution, DuoDERM® dressing, PAE 8 hydrogel, or left untreated as negative control. Both AA-Am and PAE hydrogel displayed high transparency upon application onto the wound, in contrast, DuoDERM® dressing showed partial transparency (Fig. 7A), where the opaqueness may pose challenges in wound monitoring without removing the dressing. Wound healing in PAE hydrogel group was significantly faster than control, E-F, and AA-Am groups (Fig. 7A), which was also confirmed by statistical analysis of wound areas (Fig. 7B). On day 6, the relative wound area of control group was 69.4 %, while this number was 28.9 % in PAE hydrogel group. On day 13 and day 19, the average wound areas for the control group were 25.3 % and 21.0 %, correspondingly. In comparison, PAE hydrogel group demonstrated smaller wound area at 14.8 % and 10.4 %, respectively (Fig. 7B). It's important to note that from day 13 to day 19, all groups displayed significantly reduced wound healing rates, a phenomenon attributable to the chronic nature of diabetic wounds [48]. DuoDERM® dressing is a hydrocolloid dressing specifically engineered for handling diabetic and chronic wounds, and was used as a reference standard. During the wound healing process, no significant difference of wound areas was found between PAE hydrogel and DuoDERM® group (Fig. 7A–B), indicating the effective pro-healing activity of PAE hydrogels.

The process of wound healing is intricate, necessitating the systematic coordination of various biological and cellular responses, including cell migration, re-epithelialization, collagen deposition, and remodeling [49]. To understand the pro-healing effects of PAE hydrogels, wound tissues were harvested on the day 10 and day 19 for histological analysis. On day 10, wound applied with PAE hydrogel already manifested re-epithelialization, while wound in control group did not show such progress, and other wounds were covered with scab tissues (Fig. S14A). By the day 19, all wounds showed complete re-epithelialization (Fig. 7C), with regeneration of blood vessels and skin appendages such as hair follicles, sweat glands, sebaceous glands (Fig. 7C). However, the application of PAE hydrogel was associated with the smallest wound width (Fig. 7C and E), suggesting a more rapid healing process by PAE hydrogel treatment. From Masson's Trichrome (MT) staining, compared to control group, denser collagen deposition was observed in PAE hydrogel group on both day 10 and day 19 (Fig. S14B, Fig. 7D). By day 19, the presence of newly formed blood vessels indicated the angiogenic activity within the wound tissues. Although small blood vessels were formed in the other groups, PAE hydrogel group exhibited dominant vessel size and vessel amount, with a particularly large blood vessel traversing the center of the wound (Fig. 7D).

Regenerated granulation tissue thickness on day 19 was calculated based on H&E staining, and collagen deposition in skin tissue was analyzed based on MT staining. From H&E staining, both E-F and PAE hydrogel groups showed significant increased tissue thickness when compared with the control group (Fig. 7F). This observation might be due to the therapeutic influence of EGCG, which produced a more substantial impact when be gradually released within the PAE hydrogel system (Fig. 7F). PAE hydrogel group also showed the most favorable collagen deposition rate with an average of 81.6 %, which was much higher than 50.3 % in control group (Fig. 7G). Compared to control group, the levels of collagen deposition in AA-Am group, DuoDERM® group, and PAE hydrogel group showed significant differences, whereas the change in collagen deposition was not significant in the E-F group (Fig. 7G). Comparing to the spraying of E-F, the gradual release of EGCG from PAE hydrogel provided a sustaining environment for tissue growth and collagen remodeling. These results proved the pro-healing effects of PAE hydrogel, which facilitated the regeneration of the granulation tissue, contraction of the wound, and collagen deposition.

3.12. Immunofluorescence analysis

Immunofluorescence analysis was performed to further investigate the pro-healing mechanism of PAE hydrogels. First, we evaluated the process of angiogenesis in the obtained wound tissue via CD31 staining (Fig. 8A) [32]. PAE hydrogel group showed much stronger CD31 fluorescence intensity as well as larger coverage compared to control group, while the other groups showed no obvious difference on CD31 positive area compared to control group (Fig. 8A). These results were confirmed by statistical analysis (Fig. 8D), and the CD31 coverage in PAE hydrogel group was 7.1 times higher than the control group (Fig. 8D).

We then investigated the transformative effect of PAE hydrogel on macrophage phenotypes, which are important indicators for inflammation levels [50]. When macrophages predominantly exhibit the pro-inflammatory M1 phenotype, an elevated release of inflammatory cytokines occurs, leading to tissue destruction and organ malfunction. In contrast, when the quantity of anti-inflammatory M2 phenotype macrophages augments, a greater release of anti-inflammatory cytokines and growth factors occurs, resulting in enhanced tissue regeneration. Here, immunofluorescence staining of F4/80 and CD163 was used to identify M1 and M2 macrophages, respectively (Fig. 8B). The control group primarily maintained macrophages in the M1 phenotype ($F4/80^{+}$, $CD163^{-}$), which was also found in E-F and AA-Am groups (Fig. 8B). DuoDERM® treatment groups exhibited weak fluorescence from both M1 and M2 macrophages (Fig. 8B). In contrast, with the administration of PAE hydrogel, there was a significant increase in the proportion of M2 macrophage phenotype ($F4/80^{+}$, $CD163^{+}$) (Fig. 8B). Statistical analysis revealed that only PAE hydrogel group exhibited an increased M2/M1 ratio with significant difference as compared to the control group (Fig. 8E), indicating its strong capacity to induce transformation into M2 macrophages.

Moreover, TNF-α, a potent pro-inflammatory cytokine, was stained to examine the overall inflammation level. A significant level of TNF-α was observed in the control group (Fig. 8C), in contrast, the TNF-α level with PAE hydrogel treatment was merely one tenth of the control group (Fig. 8C and F). Comparably, the spraying of E-F to the wound sites did not show a significant difference in the decrease of TNF-α level compared to the control group (Fig. 8F), probably due to the absence of wound dressing, which left the wound exposed to external infection and resulted in sustained inflammation. In summary, these results suggested that PAE hydrogel effectively enhanced wound healing process by promoting angiogenesis, and inhibiting inflammation through macrophage phenotype regulation.

Here, we successfully designed and prepared PAE hydrogel wound dressing via crosslinking of dynamic E-F crosslinker with AA-Am hydrogel network, which exhibited excellent mechanical toughness, wet adhesion, self-healing, glucose-responsive drug release, and multiple biofunctions for diabetic wound treatment. The dynamic crosslinking nature of E-F crosslinker and polyhydroxy groups of EGCG enhanced mechanical strength (Fig. 2F–K), wet adhesion (Fig. 3E) and self-healing property (Fig. 3G–I) of PAE hydrogels. In the other hand, the glucose-responsiveness of E-F crosslinker (Fig. 1A) endowed the PAE hydrogels with glucose-responsive drug releasing behavior (Fig. 4C), which effectively release more EGCG according to high glucose levels in diabetic wound environment. This method is simple and effective in integrating multiple functions together into one hydrogel system.

Compared to pure AA-Am hydrogels, PAE hydrogel showed an enhanced elongation as higher as 1005.8 % and yield-softening property (Table S3). In PAE hydrogel, the addition of E-F crosslinker formed the second interpenetrating network in the skeleton of AA-Am backbone (Fig. 1A–C). More importantly, abundant phenolic hydroxyl groups, amino groups, and carboxyl groups in PAE hydrogels attracted each other to form hydrogen bonds (Fig. 1C). Due to both radical crosslinking and the hydrogen bonding interactions, a denser physical cross-linking network was formed to dissipate energy [17], leading to the increased elongation and decreased tensile strength. Compared to previous studies on polyacrylic acid or polyacrylamide-based hydrogel systems (Table S3) [16–18], herein, PAE hydrogel demonstrated excellent toughness and the largest elongation at break. Meanwhile, as compared

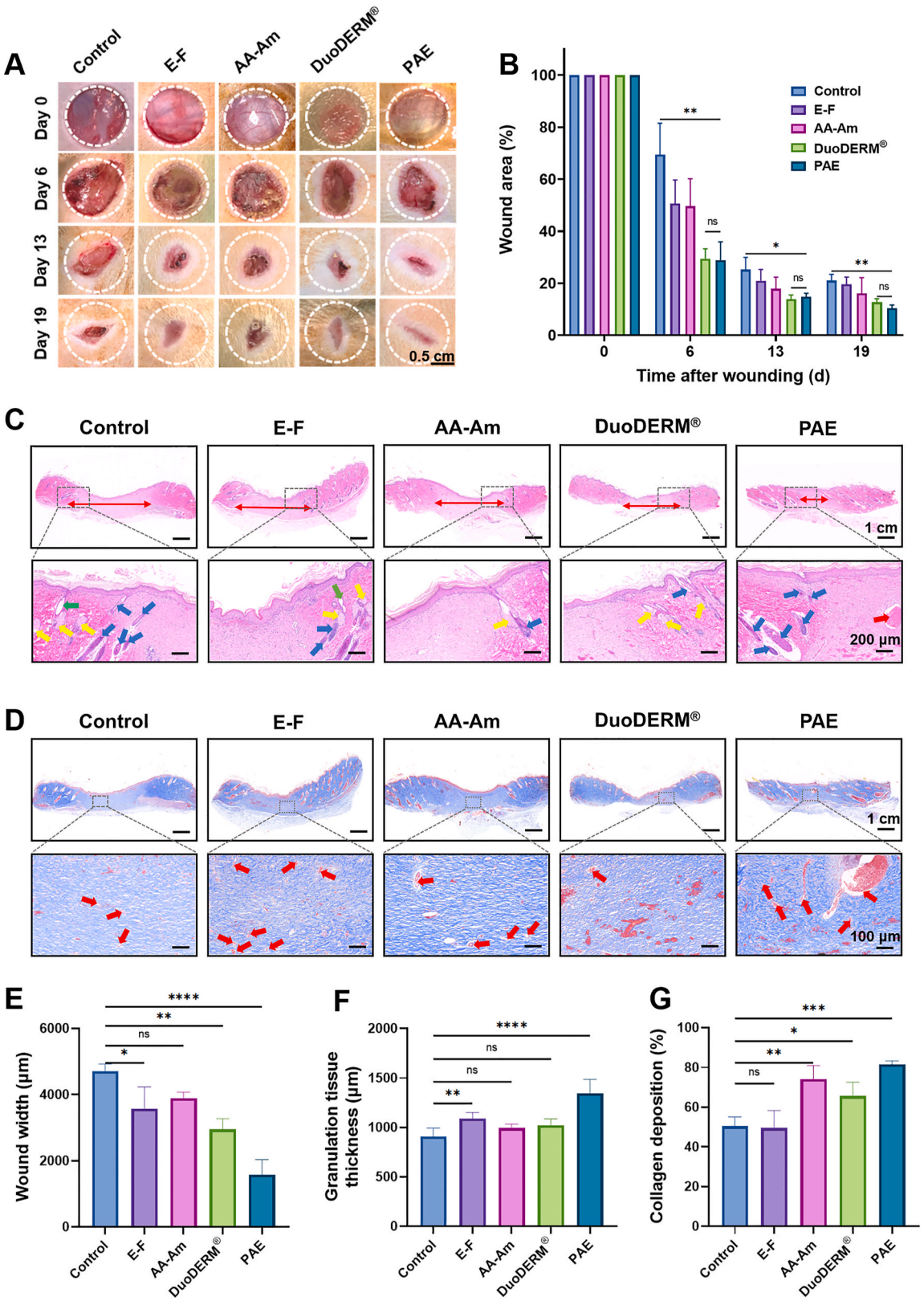

Fig. 7. Diabetic wound healing performance of PAE hydrogels. (A) Representative photograph of diabetic wounds with different treatments. (B) Quantification of wound area in each group during healing process. (C) H&E staining of wound sections on day 19. Red double-end arrows represent the range of wound areas. Blue, yellow and green arrows represent hair follicles, sebaceous glands and sweat glands, respectively. (D) Masson's trichrome (MT) staining images on day 19. Red arrows represent blood vessels. (E) Wound width in each group on day 19. (F) Thickness of epidermis granulation tissues on day 19 based on H&E staining. (G) Collagen deposition on day 19 based on MT staining. Data are shown as mean ± SD, n = 3. *p < 0.05, **p < 0.01, ***p < 0.001, ****p < 0.0001, ns means not significant (p > 0.05).

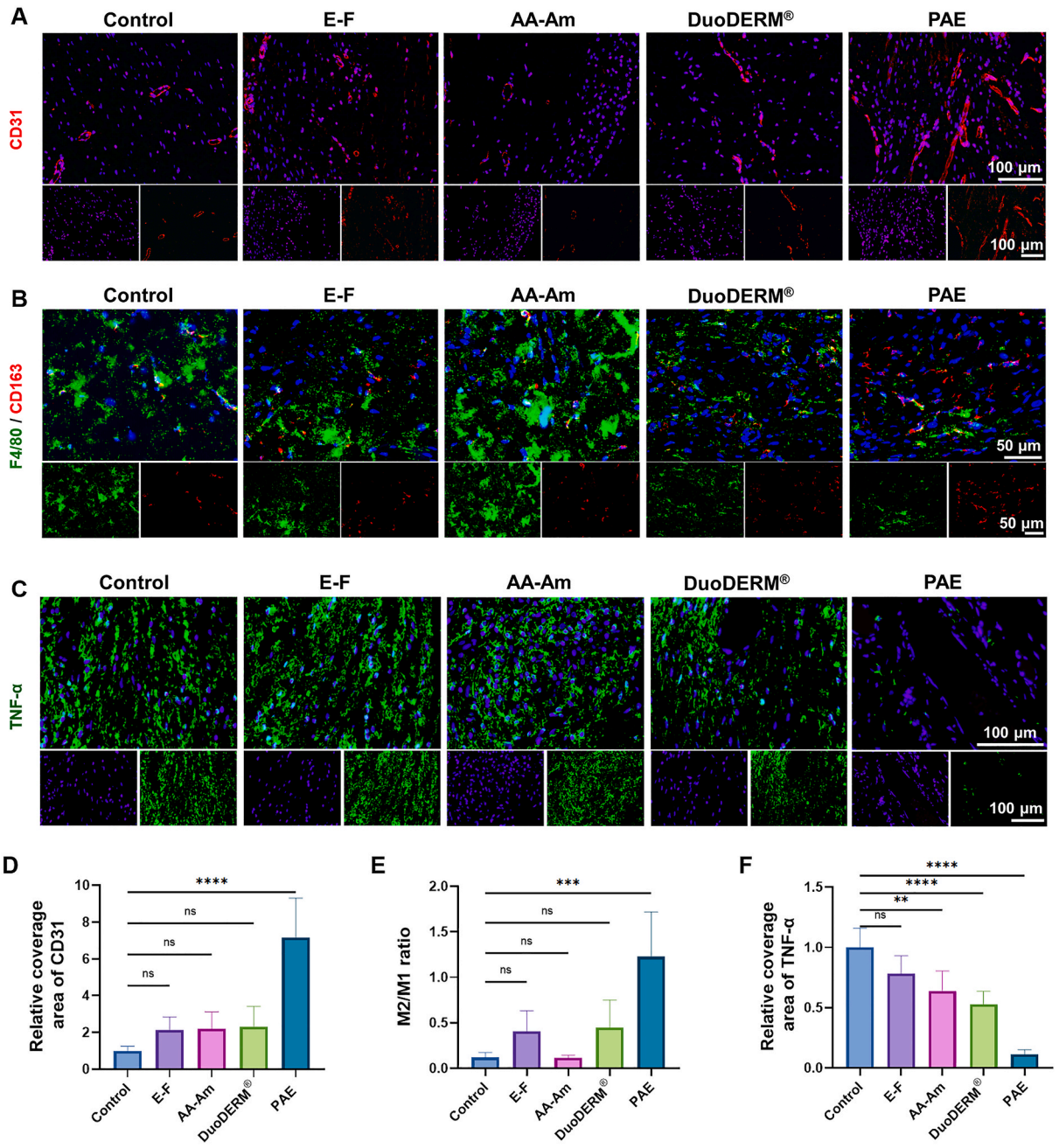

Fig. 8. Immunofluorescence staining of skin tissues post diabetic wound healing. (A) Representative images of CD31 staining (red) in wound sites on day 19. (B) Immunofluorescence images of macrophages in wound tissues stained with F4/80 (green) and CD163 (red), respectively. (C) Representative images of TNF-α staining (green) in wound sites on day 19. Nuclei were stained with DAPI (blue). (D) Quantitative analysis of relative coverage of CD31. (E) Ratio of M2 macrophages to M1 macrophages in wound tissues, which is calculated by the division of $F4/80^{+}$, $CD163^{+}$ area to $F4/80^{+}$, $CD163^{-}$ area. (F) Quantitative analysis of the relative coverage of TNF-α. Data are shown as mean ± SD (n = 5). $^{**}p < 0.01$, $^{***}p < 0.001$, $^{****}p < 0.0001$, ns means not significant ($p > 0.05$).

to previous polyacrylamide integrating with EGCG-APBA (Table S3) [23], our PAE hydrogel showed a higher tensile strength and larger elongation, with 14 % increase in tensile strength and 51 % increase in elongation at break.

Besides of flexibility, wound dressings with ideal tissue adhesion can firmly cover the wound site and provide a beneficial microenvironment during wound healing. The hydrogen bonding and polyphenol coordination bond were recognized as the major factors that contribute to the adhesive properties [15,16], as well as other covalent bonding (such as substrates containing amine or thiol groups through Schiff base or Michael addition reactions) [51]. Here, the dynamic boronic ester and hydrogen bonding not only enhanced the cohesion of the PAE hydrogel (Fig. 1C), but also improved the interface adhesion between PAE hydrogel and wet tissues (Fig. 3E–F). In addition, the abundant phenolic hydroxyl groups of EGCG (Fig. 1A) and flexible polymer chains of PAE hydrogel contributed to the high interfacial adhesion capacity. PAE hydrogels integrated with good interface adhesion, and balanced intrinsic strength, leading to outstanding tissue adhesion capability.

Self-healing of hydrogels relies on chain segment motion and dynamic bonding [52,53], which includes dynamic noncovalent bonding (such as hydrogen bonding, metal coordination, ionic interactions, etc.) [54], and dynamic covalent bonding (such as reversible boronic esters, disulfide bonds, Schiff base reactions, etc.) [55]. Here, the rapid self-healing performance of PAE hydrogels mainly resulted from the

reversible bonding of boronic esters of E-F crosslinker (Figs. 1A and 3G), as well as the abundant hydrogen bonding between E-F crosslinker and AA-Am network at the fracture interfaces (Fig. 3G), both leading to the reconstruction of the new dynamic bonds, consequently leading to the formation of a new network (Fig. 3G–H). The rapid self-healing capacity and ultra-stretchability of PAE hydrogels prolong their lifespan and improve their security of use during diabetic wound healing.

Considering the extensive tissue exudate in diabetic wound environment, management of biofluids is important to enhance diabetic wound healing [56,57]. It is hard for conventional dressings to effectively manage the excessive exudate around the wound bed, which inevitably caused infection and hindered wound healing. Here, PAE hydrogel can effectively absorb biofluids (Fig. 4A), as much as 10 times of its own weight (Fig. 4A–B), which is beneficial for removal the exudate away from the wound bed, indicating its potential for practical applications in diabetic wound healing.

In addition, PAE hydrogels released the encapsulated drugs along with the swelling in biofluids, and the drug release rate can be regulated by the concentration of E-F crosslinker (Fig. 4C) which effected the crosslinked density of the PAE hydrogel network. More interestingly, the drug release from PAE hydrogel was accelerated in high glucose solutions (Fig. 4D), due to the glucose-dependent shift in the equilibria of AFPBA molecule [34,35]. The high glucose-responsive EGCG releasing behavior made the PAE hydrogel well suitable in diabetic wound healing. When applied to the wound site, the sustained and glucose-responsive release of EGCG from PAE hydrogel exerted its effective antibacterial, antioxidative, and anti-inflammatory properties *in vitro* (Fig. 5), and therefore accelerated diabetic wound healing in rats (Fig. 7), via enhancing angiogenesis, reprogramming of macrophages, and reducing tissue-inflammatory response (Fig. 8). Besides, upon swelling and drug release of hydrogels, the inner structure of PAE hydrogels broke down with reduced amount of EGCG, which is beneficial for decreased tissue adhesion and facilitate the routine dressing change procedures.

4. Conclusion

To summarize, we successfully developed a glucose-responsive, wet-adhesive, self-healing and multi-biofunctional PAE hydrogel dressing through a straightforward process, and demonstrated its significant efficacy in promoting diabetic wound healing. PAE hydrogel was fabricated through radical copolymerization of AA-Am network and E-F crosslinker. Owing to the dynamic nature of E-F crosslinker and abundant hydrogel bonding in the network, PAE hydrogel exhibited excellent flexibility with an elongation of about 1000 %, strong tissue adhesion and promising self-healing properties. These characteristics endow the PAE hydrogel with durability during wound healing against normal body movement and external stress. Moreover, PAE hydrogel showed excellent biocompatibility, possessed anti-bacterial, antioxidative, and anti-inflammatory abilities, due to the glucose-responsive release of EGCG from the dressing. In diabetic wound model, PAE hydrogel not only accelerated the healing rate, but also enhanced the formation of granulation tissues and collagen deposition. PAE hydrogels exhibited advantageous pro-healing effect, through the promotion of angiogenesis, regulation of macrophage phenotypes from M1 to M2, and reduction of inflammation. This multifunctional hydrogel with excellent mechanical performance, wet adhesion, and self-healing ability provides a promising solution for diabetic wound treatment, and has great potential in other wound management, such as wound encapsulation, infected wounds, and surgical wounds.

CRediT authorship contribution statement

Zhuo Huang: Writing – original draft, Methodology, Investigation, Data curation, Conceptualization. **Min Wang:** Methodology, Investigation, Data curation. **Langjie Chai:** Investigation, Data curation. **Hang Chen:** Investigation, Data curation. **Danyang Chen:** Methodology, Conceptualization. **Yulin Li:** Software. **Hongtao Liu:** Methodology, Investigation. **You Wu:** Investigation. **Xuxia Yang:** Investigation. **Lu He:** Investigation. **Longjian Xue:** Supervision. **Yifeng Lei:** Writing – review & editing, Supervision, Project administration, Funding acquisition, Conceptualization. **Liang Guo:** Writing – review & editing, Supervision, Project administration, Funding acquisition.

Declaration of competing interest

The authors declare that they have no known competing financial interests or personal relationships that could have appeared to influence the work reported in this paper.

Data availability

Data will be made available on request.

Acknowledgement

This work was supported by National Natural Science Foundation of China (Nos. 81871484 and 82172096), Zhongnan Hospital Fund for Translational Medicine and Interdisciplinary Research (No. ZNJC202328), Shenzhen Science and Technology Program (No. JCYJ20220530140610022).

Appendix A. Supplementary data

Supplementary data to this article can be found online at https://doi.org/10.1016/j.mtbio.2024.101159.

References

[1] V. Falanga, Wound healing and its impairment in the diabetic foot, Lancet 366 (9498) (2005) 1736–1743.
[2] D.G. Armstrong, A.J.M. Boulton, S.A. Bus, Diabetic foot ulcers and their recurrence, N. Engl. J. Med. 376 (24) (2017) 2367–2375.
[3] J.G. Powers, C. Higham, K. Broussard, T.J. Phillips, Wound healing and treating wounds: chronic wound care and management, J. Am. Acad. Dermatol. 74 (4) (2016) 607–625.
[4] E. Everett, N. Mathioudakis, Update on management of diabetic foot ulcers, Ann. N. Y. Acad. Sci. 1411 (1) (2018) 153–165.
[5] B. Guo, R. Dong, Y. Liang, M. Li, Haemostatic materials for wound healing applications, Nat. Rev. Chem 5 (11) (2021) 773–791.
[6] Y. Xiong, Q. Feng, L. Lu, K. Zha, T. Yu, Z. Lin, Y. Hu, A.C. Panayi, V. Nosrati-Ziahmagi, X. Chu, L. Chen, M.-A. Shahbazi, B. Mi, G. Liu, Immunomodulatory hydrogels: Advanced regenerative tools for diabetic foot ulcer, Adv. Funct. Mater. 33 (10) (2023) 2213066.
[7] C. Liu, Y. Wang, P. Wang, Y. Gong, B. Yi, J. Ruan, X. Wang, In situ electrospun aloe-nanofiber membrane for chronic wound healing, Smart Mater. Med. 4 (2023) 514–521.
[8] B. Hu, M. Gao, K.O. Boakye-Yiadom, W. Ho, W. Yu, X. Xu, X.-Q. Zhang, An intrinsically bioactive hydrogel with on-demand drug release behaviors for diabetic wound healing, Bioact. Mater. 6 (12) (2021) 4592–4606.
[9] F. Huang, X. Lu, Y. Yang, Y. Yang, Y. Li, L. Kuai, B. Li, H. Dong, J. Shi, Microenvironment-based diabetic foot ulcer nanomedicine, Adv. Sci. 10 (2) (2023) e2203308.
[10] S.H.S. Dananjaya, N. Bandara, I.M.N. Molagoda, W.M.G. Sandamalika, D. Kim, N. Ganepola, A.P. Attanayake, D. Choi, Multifunctional alginate/polydeoxyribonucleotide hydrogels for promoting diabetic wound healing, Int. J. Biol. Macromol. 257 (2024) 128367.
[11] T. Xiang, Q. Guo, L. Jia, T. Yin, W. Huang, X. Zhang, S. Zhou, Multifunctional hydrogels for the healing of diabetic wounds, Adv. Healthcare Mater. 13 (2024) 2301885.
[12] W. Zhang, K. Zha, Y. Xiong, W. Hu, L. Chen, Z. Lin, C. Yu, W. Zhou, F. Cao, H. Hu, B. Mi, G. Liu, Glucose-responsive, antioxidative HA-PBA-FA/EN106 hydrogel enhanced diabetic wound healing through modulation of FEM1b-FNIP1 axis and promoting angiogenesis, Bioact. Mater. 30 (2023) 29–45.
[13] Y. Yang, M. Li, G. Pan, J. Chen, B. Guo, Multiple stimuli-responsive nanozyme-based cryogels with controlled no release as self-adaptive wound dressing for infected wound healing, Adv. Funct. Mater. 33 (31) (2023) 2214089.
[14] H. Chen, Y. Cheng, J. Tian, P. Yang, X. Zhang, Y. Chen, Y. Hu, J. Wu, Dissolved oxygen from microalgae-gel patch promotes chronic wound healing in diabetes, Sci. Adv. 6 (20) (2020) eaba4311.
[15] Y.N. Jiang, X. Zhang, W. Zhang, M.H. Wang, L.W. Yan, K.F. Wang, L. Han, X. Lu, Infant skin friendly adhesive hydrogel patch activated at body temperature for

bioelectronics securing and diabetic wound healing, ACS Nano 16 (6) (2022) 8662–8676.
[16] L. Wang, L. Duan, G. Liu, J. Sun, M.A. Shahbazi, S.C. Kundu, R.L. Reis, B. Xiao, X. Yang, Bioinspired polyacrylic acid-based dressing: wet adhesive, self-healing, and multi-biofunctional coacervate hydrogel accelerates wound healing, Adv. Sci. 10 (16) (2023) 2207352.
[17] K. Zheng, Y. Tong, S. Zhang, R. He, L. Xiao, Z. Iqbal, Y. Zhang, J. Gao, L. Zhang, L. Jiang, Y. Li, Flexible bicolorimetric polyacrylamide/chitosan hydrogels for smart real-time monitoring and promotion of wound healing, Adv. Funct. Mater. 31 (34) (2021) 2102599.
[18] H. Liu, Y. Wang, Z. Shi, D. Tan, X. Yang, L. Xiong, G. Li, Y. Lei, L. Xue, Fast self-assembly of photonic crystal hydrogel for wearable strain and temperature sensor, Small Methods 6 (7) (2022) 2200461.
[19] G. Sennakesavan, M. Mostakhdemin, L.K. Dkhar, A. Seyfoddin, S.J. Fatihhi, Acrylic acid/acrylamide based hydrogels and its properties - a review, Polym. Degrad. Stabil. 180 (2020) 109308.
[20] H. Lee, S.M. Dellatore, W.M. Miller, P.B. Messersmith, Mussel-inspired surface chemistry for multifunctional coatings, Science 318 (5849) (2007) 426–430.
[21] S. Singla, G. Amarpuri, N. Dhopatkar, T.A. Blackledge, A. Dhinojwala, Hygroscopic compounds in spider aggregate glue remove interfacial water to maintain adhesion in humid conditions, Nat. Commun. 9 (1) (2018) 1890.
[22] H. Yuk, J. Wu, T.L. Sarrafian, X. Mao, C.E. Varela, E.T. Roche, L.G. Griffiths, C. S. Nabzdyk, X. Zhao, Rapid and coagulation-independent haemostatic sealing by a paste inspired by barnacle glue, Nat. Biomed. Eng. 5 (10) (2021) 1131–1142.
[23] X. Zhao, D. Pei, Y. Yang, K. Xu, J. Yu, Y. Zhang, Q. Zhang, G. He, Y. Zhang, A. Li, Y. Cheng, X. Chen, Green tea derivative driven smart hydrogels with desired functions for chronic diabetic wound treatment, Adv. Funct. Mater. 31 (18) (2021) 2009442.
[24] M. Shin, E. Park, H. Lee, Plant-inspired pyrogallol-containing functional materials, Adv. Funct. Mater. 29 (43) (2019) 1903022.
[25] N. Li, Y. Li, Z. Cheng, Y.D. Liu, Y.H. Dai, S. Kang, S.S. Li, N.S. Shan, S.Y. Wai, A. Ziaja, Y.F. Wang, J. Strzalka, W. Liu, C. Zhang, X.D. Gu, J.A. Hubbell, B.Z. Tian, S.H. Wang, Bioadhesive polymer semiconductors and transistors for intimate biointerfaces, Science 381 (6658) (2023) 686–693.
[26] H. Wang, X. Yi, T. Liu, J. Liu, Q. Wu, Y. Ding, Z. Liu, Q. Wang, An integrally formed Janus hydrogel for robust wet-tissue adhesive and anti-postoperative adhesion, Adv. Mater. 35 (23) (2023) 2300394.
[27] H. Yuk, C.E. Varela, C.S. Nabzdyk, X. Mao, R.F. Padera, E.T. Roche, X. Zhao, Dry double-sided tape for adhesion of wet tissues and devices, Nature 575 (7781) (2019) 169–174.
[28] K. Li, G. Xiao, J.J. Richardson, B.L. Tardy, H. Ejima, W. Huang, J. Guo, X. Liao, B. Shi, Targeted therapy against metastatic melanoma based on self-assembled metal-phenolic nanocomplexes comprised of green tea catechin, Adv. Sci. 6 (5) (2019) 1801688.
[29] X. Zan, D. Yang, Y. Xiao, Y. Zhu, H. Chen, S. Ni, S. Zheng, L. Zhu, J. Shen, X. Zhang, Facile general injectable gelatin/metal/tea polyphenol double nanonetworks remodel wound microenvironment and accelerate healing, Adv. Sci. 11 (9) (2024) 2305405.
[30] Z. Guo, H. Liu, Z. Shi, L. Lin, Y. Li, M. Wang, G. Pan, Y. Lei, L. Xue, Responsive hydrogel-based microneedle dressing for diabetic wound healing, J. Mater. Chem. B 10 (18) (2022) 3501–3511.
[31] G. Bao, Q. Gao, M. Cau, N. Ali-Mohamad, M. Strong, S. Jiang, Z. Yang, A. Valiei, Z. Ma, M. Amabili, Z.-H. Gao, L. Mongeau, C. Kastrup, J. Li, Liquid-infused microstructured bioadhesives halt non-compressible hemorrhage, Nat. Commun. 13 (1) (2022) 5035.
[32] Z. Shao, T. Yin, J. Jiang, Y. He, T. Xiang, S. Zhou, Wound microenvironment self-adaptive hydrogel with efficient angiogenesis for promoting diabetic wound healing, Bioact. Mater. 20 (2023) 561–573.
[33] W. Xie, W. Hu, Z. Huang, M. Li, H. Zhang, X. Huang, P. Yao, Betulinic acid accelerates diabetic wound healing by modulating hyperglycemia-induced oxidative stress, inflammation and glucose intolerance, Burns Trauma 10 (2022) tkac007.
[34] L. Liu, X. Tian, Y. Ma, Y. Duan, X. Zhao, G. Pan, A versatile dynamic mussel-inspired biointerface: from specific cell behavior modulation to selective cell isolation, Angew. Chem. Int. Ed. 57 (26) (2018) 7878–7882.
[35] Y. Ma, P. He, W. Xie, Q. Zhang, W. Yin, J. Pan, M. Wang, X. Zhao, G. Pan, Dynamic Colloidal Photonic Crystal Hydrogels with Self-Recovery and Injectability, vol. 2021, 2021 9565402. Research.
[36] D.H. Chou, M.J. Webber, B.C. Tang, A.B. Lin, L.S. Thapa, D. Deng, J.V. Truong, A. B. Cortinas, R. Langer, D.G. Anderson, Glucose-responsive insulin activity by covalent modification with aliphatic phenylboronic acid conjugates, Proc. Natl. Acad. Sci. U.S.A. 112 (8) (2015) 2401–2406.
[37] R. Pinnataip, B.P. Lee, Oxidation chemistry of catechol utilized in designing stimuli-responsive adhesives and antipathogenic biomaterials, ACS Omega 6 (8) (2021) 5113–5118.
[38] Y. Chen, Q. Li, Y. Li, Q. Zhang, J. Huang, Q. Wu, S. Wang, Fabrication of cellulose nanocrystal-g-poly(acrylic acid-co-acrylamide) aerogels for efficient Pb(II) removal, Polymers 12 (2) (2020) 333.
[39] Y. Wang, L.R. Shang, G.P. Chen, L.Y. Sun, X.X. Zhang, Y.J. Zhao, Bioinspired structural color patch with anisotropic surface adhesion, Sci. Adv. 6 (4) (2020) eaax8258.
[40] Y. Wei, Y.Y. He, C.Y. Wang, G. Chen, B.X. Zhao, Asymmetric "Janus" biogel for human-machine interfaces, Adv. Funct. Mater. 33 (34) (2023) 2214366.
[41] Y. Li, Z. Yang, Q. Sun, R. Xu, R. Li, D. Wu, R. Huang, F. Wang, Y. Li, Biocompatible cryogel with good breathability, exudate management, antibacterial and immunomodulatory properties for infected diabetic wound healing, Adv. Sci. 10 (31) (2023) e2304243.
[42] M. Caprioli, I. Roppolo, A. Chiappone, L. Larush, C.F. Pirri, S. Magdassi, 3D-printed self-healing hydrogels via digital light processing, Nat. Commun. 12 (1) (2021) 2462.
[43] Z.H. Li, Y. Zhao, H.W. Huang, C.R. Zhang, H. Liu, Z.H. Wang, M.J. Yi, N. Xie, Y. L. Shen, X.Z. Ren, J.C. Wang, J.W. Wang, A nanozyme-immobilized hydrogel with endogenous ROS-scavenging and oxygen generation abilities for significantly promoting oxidative diabetic wound healing, Adv. Healthcare Mater. 11 (22) (2022) e2201524.
[44] L. Qiao, Y. Liang, J. Chen, Y. Huang, S.A. Alsareii, A.M. Alamri, F.A. Harraz, B. Guo, Antibacterial conductive self-healing hydrogel wound dressing with dual dynamic bonds promotes infected wound healing, Bioact. Mater. 30 (2023) 129–141.
[45] B. Hu, Y. Shen, J. Adamcik, P. Fischer, M. Schneider, M.J. Loessner, R. Mezzenga, Polyphenol-binding amyloid fibrils self-assemble into reversible hydrogels with antibacterial activity, ACS Nano 12 (4) (2018) 3385–3396.
[46] C. Chai, P. Zhang, L. Ma, Q. Fan, Z. Liu, X. Cheng, Y. Zhao, W. Li, J. Hao, Regenerative antibacterial hydrogels from medicinal molecule for diabetic wound repair, Bioact. Mater. 25 (2023) 541–554.
[47] J. Wei, W. Zhang, X. Mou, H. Meng, Q. Ma, W. Wang, X. Li, Q. Tu, W. Tian, N. Huang, Z. Yang, Bioinspired hemostatic and anti-infective armor for wound healing assisted by metal-phenol-polyamine system, Adv. Funct. Mater. 34 (2024) 2306267.
[48] J.B. Cole, J.C. Florez, Genetics of diabetes mellitus and diabetes complications, Nat. Rev. Nephrol. 16 (7) (2020) 377–390.
[49] M.G. Monaghan, R. Borah, C. Thomsen, S. Browne, Thou shall not heal: overcoming the non-healing behaviour of diabetic foot ulcers by engineering the inflammatory microenvironment, Adv. Drug Deliv. Rev. 203 (2023) 115120.
[50] Y.J. Fu, Y.F. Shi, L.Y. Wang, Y.F. Zhao, R.K. Wang, K. Li, S.T. Zhang, X.J. Zha, W. Wang, X. Zhao, W. Yang, All-natural immunomodulatory bioadhesive hydrogel promotes angiogenesis and diabetic wound healing by regulating macrophage heterogeneity, Adv. Sci. 10 (13) (2023) e2206771.
[51] X. Zhao, Y. Liang, Y. Huang, J. He, Y. Han, B. Guo, Physical double-network hydrogel adhesives with rapid shape adaptability, fast self-healing, antioxidant and NIR/pH stimulus-responsiveness for multidrug-resistant bacterial infection and removable wound dressing, Adv. Funct. Mater. 30 (17) (2020) 1910748.
[52] B. Li, P.-F. Cao, T. Saito, A.P. Sokolov, Intrinsically self-healing polymers: from mechanistic insight to current challenges, Chem. Rev. 123 (2) (2023) 701–735.
[53] Z. Li, J. Lu, T. Ji, Y. Xue, L. Zhao, K. Zhao, B. Jia, B. Wang, J. Wang, S. Zhang, Z. Jiang, Self-healing hydrogel bioelectronics, Adv. Mater. 36 (21) (2024) 2306350.
[54] Y. Wang, X. Huang, X. Zhang, Ultrarobust, tough and highly stretchable self-healing materials based on cartilage-inspired noncovalent assembly nanostructure, Nat. Commun. 12 (1) (2021) 1291.
[55] Y. Liang, Z. Li, Y. Huang, R. Yu, B. Guo, Dual-dynamic-bond cross-linked antibacterial adhesive hydrogel sealants with on-demand removability for post-wound-closure and infected wound healing, ACS Nano 15 (4) (2021) 7078–7093.
[56] F. Bao, G. Pei, Z.C. Wu, H. Zhuang, Z.W.B. Zhang, Z.G. Huan, C.T. Wu, J. Chang, Bioactive self-pumping composite wound dressings with micropore array modified Janus membrane for enhanced diabetic wound healing, Adv. Funct. Mater. 30 (49) (2020) 2005422.
[57] B. Xu, A. Li, R. Wang, J. Zhang, Y. Ding, D. Pan, Z. Shen, Elastic Janus film for wound dressings: unidirectional biofluid transport and effectively promoting wound healing, Adv. Funct. Mater. 31 (41) (2021) 2105265.